Desalination and Water Treatment
www.deswater.com
doi: 10.1080/19443994.2013.874132

52 (2014) 1217–1249
February

Taylor & Francis
Taylor & Francis Group

Review: ultrasonic characterization of membranes

Elmira Kujundzic[a], Alan R. Greenberg[a,*], Michael Peterson[b]

[a]*Department of Mechanical Engineering, NSF Center for Membrane Science, Engineering and Technology, University of Colorado, Boulder, CO 80309-0427, USA*
Tel. +1-303-492-6613; Fax: +1-303-492-4637; email: alan.greenberg@colorado.edu
[b]*Department of Mechanical Engineering, University of Maine, Orono, ME 04469, USA*

Received 18 August 2013; Accepted 5 November 2013

ABSTRACT

This review describes the use of ultrasonic reflectometry (UR) for characterizing membranes and membrane processes. A growing body of literature documents the capabilities of UR as a versatile nondestructive, noninvasive, real-time, and low-cost methodology that can provide important information about a wide range of membrane-based separations. A compact but thorough explanation of the ultrasonic measurement concepts relevant for use of the methodology for membrane applications is first presented. This section is followed by a description of the many studies in which UR has been employed for characterization of membrane structure, formation, compaction, and inorganic and organic membrane fouling, the latter in both real-time and post-mortem modes. Examples of recent work that incorporates the innovative use of UR for scaling in nanofiltration and reverse osmosis applications as well as results that suggest the potential of the ultrasonic slow wave to monitor pore closure in early-stage fouling are then highlighted. UR is then compared with other techniques for fouling detection so that the advantages and limitations of UR can be placed in proper perspective. Finally, valuable future directions for the incorporation of UR in membrane research, development, and practice are considered.

Keywords: Ultrasonic reflectometry; Membrane characterization; Membrane fouling; Real-time studies

1. Introduction

1.1. Importance of membrane characterization

Membrane characterization is an essential component of membrane research and development because the initial design and subsequent optimization of membrane materials, processes, and systems depend on accurate data obtained under relevant conditions. Indeed, there are countless citations in the membrane literature that deal with the myriad aspects of characterization. Nonetheless, there is a continuing need for improved characterization techniques that can be appropriately adapted for measurements from bench scale to commercial scale.

1.2. Rationale for use of ultrasonic measurement of membrane phenomena

Ideally, characterization methods should be well matched to the phenomena that they measure. In

*Corresponding author.

many cases, there are significant advantages for methods that are nondestructive, noninvasive, real time, rapid, and inexpensive to employ. Ultrasonic characterization possesses these attributes and thus represents a well-established field encompassing a wide range of engineering applications. Consequently, it should not be surprising that the advantages of such methodology for use in membrane studies were recognized almost two decades ago by Hoest et al. who described in 1994 the application of ultrasonic time-domain reflectometry (UTDR) for quantifying membrane compaction [1]. This work was followed by Bond et al. who first proposed the use of UTDR for the study of membrane fouling in 1995 [2]. Although still a relatively specialized methodology, a robust literature has arisen in this area. Thus, the goal of this review is to provide an overview of developments in the use of ultrasonics for membrane and membrane-processes characterization as well as to highlight a few recent innovative approaches of this methodology.

1.3. Scope of this review

This review builds upon and expands the previous effort by Krantz and Greenberg [3] and is organized as follows. Section 2 provides an appropriately detailed description of ultrasonic measurement concepts that are relevant for membrane applications. Section 3 summarizes the growing literature on the use of ultrasonics for a range of membrane characterization applications including structure and formation, creep (compaction), and inorganic and organic membrane fouling, the latter in both real-time and post-mortem modes. Section 4 reviews recent and innovative work that highlights the use of ultrasonics for scaling measurement during nanofiltration (NF) with internally situated ultrasonic transducers, for the development of ultrasonic sensors as active elements for automatic control of fouling via flow reversal (FR), and initial studies using the slow wave to quantify permeation changes due to fouling. Section 5 compares ultrasonic reflectometry (UR) with other approaches to membrane fouling so that the advantages and limitations of UR can be placed into proper perspective. Possible future directions for membrane ultrasonics are then considered in section 6. Since the work described in these sections utilizes the time domain or the frequency domain of waves reflected from an interface of interest, the terms UTDR and ultrasonic frequency-domain reflectometry (UFDR) are used throughout. A more generic but quite appropriate treatment is to group these via the term UR.

2. Ultrasonic measurement concepts

The characterization and monitoring of membranes through the use of ultrasonic measurements is based on extensive literature in the field of acoustics [4,5] and a related literature in elasto-dynamics or waves in solids as well [6–8]. To date the literature on membrane characterization has made use of frequencies which are above the audible range for humans, approximately 20 kHz. In all of the published work, the frequencies employed for testing and monitoring are well above the audible range, in the same range used for medical diagnostic ultrasound. Therefore, without a loss of generality, the acoustic monitoring of membranes will be referred to as ultrasonic waves. However, a clear distinction should be made from ultrasonic cleaning which occurs at higher intensities and lower frequencies. Ultrasound used for cleaning, which is similar to medical therapy applications, is usually performed using lower frequencies of 25–50 kHz with intensities of 0.1–10 W/cm^2. The high intensity applications contrast with the monitoring or diagnostics applications which are performed at frequencies in the MHz range and intensities on the order of a few mW/cm^2. The latter intensity and frequencies will be considered for the monitoring of separation processes with the understanding that while safety issues should always be considered, the safety concerns are generally limited to both higher intensities and lower frequencies than those typically used for ultrasonic monitoring applications [9].

The manner in which the membrane responds to the ultrasonic wave is dependent on the mechanisms of the separation processes and the associated membrane structure. In particular, while the theoretical framework for waves in porous materials [10] is applicable to microporous membranes in which the fluid permeates the pores, a reverse osmosis (RO) membrane would respond in a manner which is consistent with dense materials. The elastic properties of a similar dense material can be used for modeling of waves impinging normal to a solid fluid-loaded thin plate. In both cases, the wave is assumed to be normal to the plane of the membrane and the radius of curvature is assumed to be larger relative to the spot size of the ultrasonic transducer. The exception would be for cases where the generation of a plate wave is used to inspect a larger area of the membrane [11,12]. The plate wave is typically generated either through the use of a custom transducer or else through the use of a transducer which is coupled through a fluid to the plate materials at an angle that is far from normal incidence. Therefore, to understand the limiting cases for the applicability of these theories, it is necessary to

develop a more general framework. More specific cases can thus be better understood from the general theory. In Fig. 1, the first characteristic that must be considered in performing modeling of the reflection from a membrane is based on the existence of the slow wave in the material. The slow wave is dependent on the pore size to wavelength ratio as well as the viscosity of the fluid. The viscosity of the fluid can present challenges for a number of important separations since temperature of the fluid can vary widely, which may result in the need to perform more complex analysis of the wave propagation for some configurations even though the applicability of the more complex analysis may not always be required. If the slow wave is generated, then the frequency transition may determine the response of the membrane to fouling. Even when the slow wave is not generated, it is important to recognize that the type of foulant can significantly influence the response of the membrane to fouling. For example, for a membrane where the slow wave is not generated in the pores of the membrane, the presence of an inorganic and an organic foulant may have the opposite effect on the reflection coefficient from the interface. The inorganic scalant has a reflection coefficient that can be higher than the basic membrane with an organic foulant serving as an impedance matching layer between the fluid and the membrane. The impedance matching layer can reduce the reflection coefficient from the membrane surface. Finally, in all cases, the reflection of the front faces of nearly all membranes will superpose on the back-face reflection. This so called thin plate problem has been considered for both the forward and inverse problem elsewhere and is, in general, reasonably tractable [13,14]. However, the analysis needs to be performed in a way that the front face can be separated either through deconvolution, cepstral, or other techniques [15,16].

From the framework in Fig. 2 and the following section, the conditions under which more complex modeling is required can be identified. In contrast, for some conditions, a simplified analysis is sufficient. The most general solution to the problem is required for those conditions when the pore size is sufficiently large that a slow wave can be generated and the damping of the polymeric membrane is a significant factor. A dense fouling layer on a material with small pore diameters in the material and with low material damping such as some highly cross-linked polymers or a ceramic is amenable to the simpler analysis. The

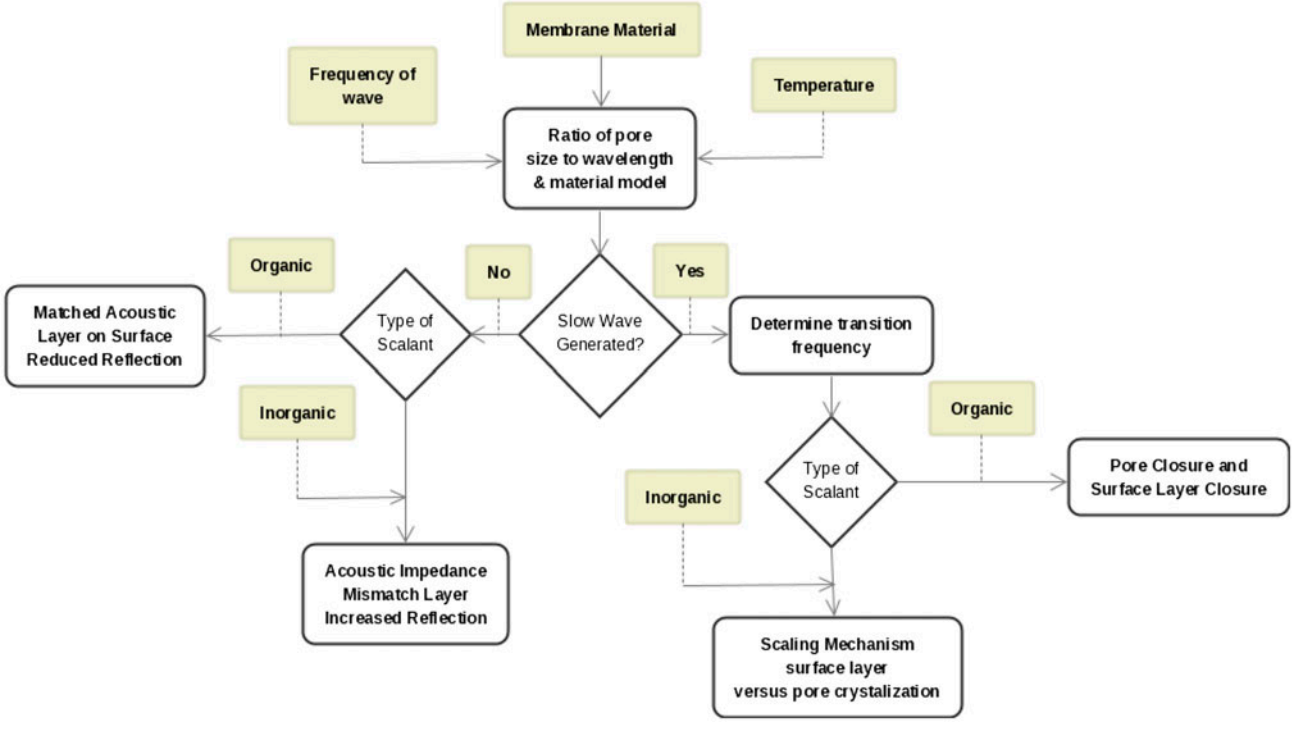

Fig. 1. The modeling of the reflection of an ultrasonic wave from a porous membrane should consider both the potential for the propagation of a slow wave in the fluid in the pores as well as the type of foulant. In nearly all cases, the reflection is from a thin layer, and the back-wall and front-wall reflections will overlap.

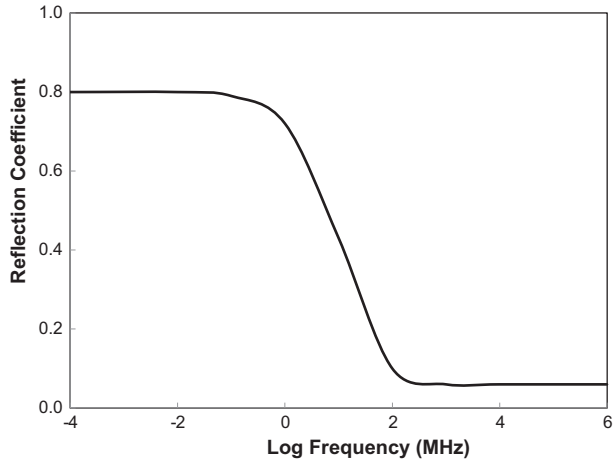

Fig. 2. The magnitude of the reflection from a porous interface is dependent upon the generation of a slow wave in the porous material. The change in frequency results in a change in reflection coefficient.

description of waves in porous material will start with the simple case and add complexity.

2.1. Waves in fluids, solids, and porous solids

For the most general case of ultrasonic waves in a membrane, it is assumed that the shear modulus of the membrane material is characteristic of a solid material. Initially, the equations of motion can be expressed for elastic materials in a manner which is characteristic of ceramic membranes where material damping is negligible. This model should first be extended to account for the effect of the inelastic characteristics of a polymeric membrane. To this model is then added the effect of fluid-saturated pores. This would best represent those membranes where the pores are of sufficient size to allow fluid flow with the effects of fluid viscosity altering the effective pore diameter. The viscoelastic response, which is more representative of polymeric membranes, should also be considered as well as the existence of fluid viscosity in both the feed and permeate solutions.

In order to understand the reflection of the wave from the membrane surface, it is necessary to recognize that the interaction of the wave with the membrane is dependent on the relative elastic properties of the fluid and the solid. From this dependence, the concept of acoustic impedance then allows the response of the materials to insonification of the surface to be understood. The complex nature of a porous viscoelastic medium requires an incremental approach to understanding the factors responsible for the reflection from the membrane surface.

The first solution to the wave equation is familiar from acoustics in a fluid medium. The direction of propagation of the wave is in the same direction as the displacement, and it is referred to as either a longitudinal or a pressure wave. The wave propagates at a velocity that depends on the elastic properties of

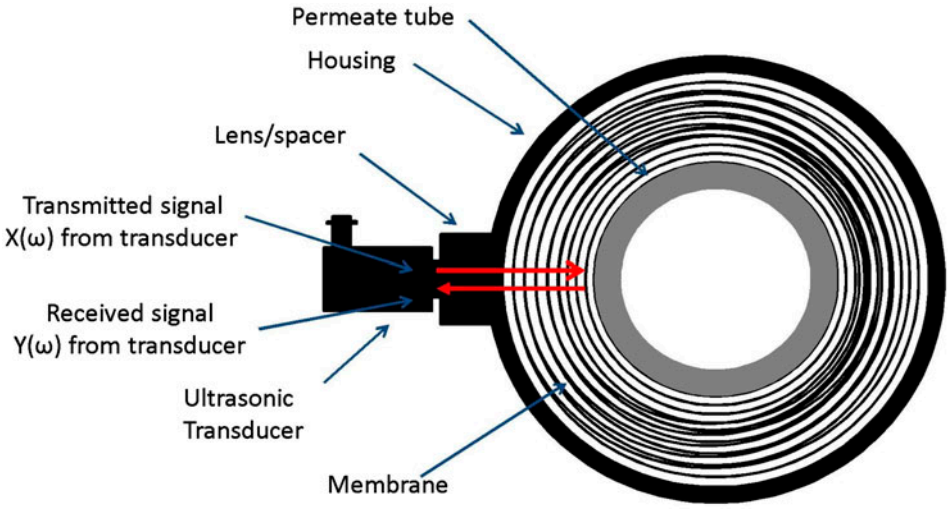

Fig. 3. For the spiral-wound configuration shown, the signal generated from the ultrasonic transducer is convolved with the response from the wall of the module, the transmission coefficient from the wall to the fluid, the response of the fluid surrounding the membrane, and the reflection from the membrane. The return path results in the response in the opposite direction including the response of the fluid and the module wall as well as the transmission coefficient from the fluid to the wall.

the medium. The elastic properties of the medium are defined as Lame's constant (λ') and the shear modulus (μ) where:

$$\lambda' = \frac{Ev}{(1+v)(1-2v)} \quad \text{and} \quad \mu = \frac{E}{2(1+v)} \tag{1}$$

and E and v are Young's modulus and Poisson's ratio, respectively [17]. Then in terms of Lame's constants, we can express the velocity of the longitudinal wave in a material where the lateral boundaries are far from the disturbance (such as a wave which is normal to the separation surface of a membrane) as:

$$C_L = \sqrt{\frac{\lambda' + 2\mu}{\rho}} \tag{2}$$

where ρ is the density of the material (medium).

This can be shown to give the velocity in a fluid which is typically written as:

$$C = \sqrt{\frac{B}{\rho}} \tag{3}$$

where the velocity C is for the only wave which will propagate in an inviscid fluid, i.e. the longitudinal wave, and B, the bulk modulus, is defined as:

$$B = \lambda' + \frac{2\mu}{3} \tag{4}$$

For water, the velocity of the wave in the fluid is given by:

$$c = 1449 + 4.9T + 0.055T^2 + 0.003T^3 + (1.39 - 0.012T)(s-35) + 0.17p \tag{5}$$

where T is the temperature in ˚C, s is the salinity in parts per thousand and p is pressure in kPa.

This wave should be distinguished from the shear wave which occurs in solid materials. The transverse or shear wave propagates at lower velocity than the longitudinal wave. The velocity of propagation of the shear wave, C_S, is a function of the shear modulus and the density of the material:

$$C_S = \sqrt{\frac{\mu}{\rho}} \tag{6}$$

The shear wave is physically distinct from the longitudinal wave since the displacement is orthogonal to the propagation direction. In order to resolve the general stress field on a free surface, it is clear that not only the normal stresses associated with the longitudinal wave are required, but the transverse wave with displacement normal to the propagation direction is also required. The shear wave is generated by either a specific type of physical excitation of the surface, or it is a result of the generation of this shear wave to satisfy the boundary conditions for a nonnormal incident angle. For the assumptions of normal incidence and a large radius of curvature typical of membrane inspection, the shear wave will not be generated.

In this material model, the assumption is for a linear elastic response of the material. This is a reasonable assumption for a wide range of loads and frequencies in a ceramic material such as those used in some high temperature and corrosive separation processes. However, the vast majority of the modern commercial membrane processes are performed using polymeric membranes. For these polymeric membranes, the consequences of material damping cannot be ignored, and analysis of the signals should be performed in a fashion that recognizes the effect of both wave frequency (and time) and temperature on the response of the membrane. The simplest implementation of the damping is with a complex modulus or a simple decay term in the solution to the wave equation. For example, if a solution to the wave equation corresponds to a wave traveling in an elastic medium in the x direction, the displacement u has the form of:

$$u = Ae^{i\omega\left(\frac{x}{C} - t\right)} \tag{7}$$

where A is the amplitude of the wave, t is time, and ω is the radial or angular frequency. When damping is introduced, the amplitude simply decays at α as a function of time, $e^{-\alpha t}$. This loss mechanism is a reasonable model for the response of polymers. The wavelength of the ultrasonic wave λ is found from the frequency and velocity C in the medium:

$$\lambda = \frac{C}{\omega} = \frac{C}{2\pi f} \tag{8}$$

where f is the ordinary frequency. If the problem is subjected to a more rigorous analysis, the result will be a nonlinear response (e.g. [18]) which is beyond the scope of the current discussion. However, from a strictly pragmatic perspective, these effects are critical to include in the formulation of the analysis of the materials response. The final confounding effect in these materials is the existence of a response that is specifically associated with the material permeability.

The final wave type, which exists only in a porous material, is the slow wave. First described in the form of a semi-phenomenological model by Biot, the formulation was developed for both low-frequency [19], and high-frequency cases [20], which were later

experimentally verified [21]. The model by Biot considers the solution of the longitudinal wave in fluid-saturated porous materials in which a wave is generated in the form of the fluid contained within the porous solid material. When the wave in the solid is in phase with the wave in the fluid, the velocity is closely related to a mixture of the response of the solid and the liquid. However, with a two-phase material, the potential exists to generate a wave in which the fluid motion is out of phase with the solid motion or a sloshing wave. The velocity of the slow wave is a function of the density of both the fluid and solid:

$$C_{SL} = f(\rho_f, \rho_s, \phi, \lambda_s, \mu_s, B_f, \upsilon_f) \tag{9}$$

where ρ_f and ρ_s are the density of the fluid and solid, respectively, ϕ is the permeability of the solid and λ_s and μ_s are the Lame constants of the solid frame, and B_f and υ_f are the bulk density and viscosity of the fluid. While the relationship of the velocity and the large number of variables makes the determination of the wave speed of the slow wave somewhat complex, conceptually the slow wave represents another factor which must be considered when determining which effects can be detected in ultrasonic measurements from a porous membrane. One of the most important recent developments related to the slow wave is the use of the critical frequency for the analysis of the fouling of porous interfaces. This is discussed in section 4.3 where the slow wave is used to detect fouling in applications where a simple interpretation of ultrasonic reflections suggests that the changes in material properties would not otherwise be detected.

A significant difficulty in studying or utilizing slow waves is that the slow wave is not readily detectable. A particularly important description of the interaction of the slow wave with a porous interface is contained in the critical wave number, k_{cr}. Below the critical wave number, the slow wave is highly attenuated since the skin depth of the fluid in the pores is large relative to the pore size. Ideally, k_{cr} represents a bifurcation below which the slow wave does not propagate [22]. Because of the dependence of the slow wave on the motion of the fluid, the detection of the critical wave number provides a basis for measuring the dynamic interaction between the matrix and the pore fluid [23]:

$$k_{cr} = y\frac{\pi\varpi}{\rho_0^S C^S} \tag{10}$$

where y is a term which combines material properties and ϖ is a parameter which characterizes the porous structure, and which are defined as:

$$y = y(\rho_0^S, \rho_0^F, C^S, C) \tag{11}$$

Here, ρ_0^S and ρ_0^F represent the partial mass densities of the solid and fluid, respectively. C^S is the velocity of the longitudinal wave in the skeleton, and C is the wave speed in the fluid. In addition, ϖ is related to the porosity n_0, viscosity of the fluid υ_f, and permeability of the porous medium ϕ by:

$$\varpi = \frac{n_0\upsilon_f}{\phi} \tag{12}$$

While the relationship is complex, the physical relationship which determines the frequency at which the critical wave propagates is more straightforward. Above the critical frequency, the skin depth of the fluid in the pores is sufficiently thick relative to the pore diameter that out-of-phase motion of the fluid in the pores relative to the solid frame occurs. While mathematically this is a single value, the actual measurements and a more sophisticated analysis show something which more closely approximates a relaxation curve [24]. The effect of viscosity which alters the skin depth or the effective diameter of the fluid-filled pores as well as the change in frequency can be seen to create the transition from both theory and experiment. In a typical membrane application, the effective change over time to a membrane in use is minimal for all of the variables associated with the calculation of the critical frequency with the exception of the permeability of the porous medium. Unlike simple measurements of reflection coefficient, which depend on a change in the average ultrasonic properties at the membrane material interface, the critical frequency measurement is sensitive to permeability of the interface and is generally insensitive to other properties of the materials [23]. Other methods are sensitive to the properties of the fouling layer, but the slow-wave measurement technique is sensitive to permeability changes regardless of the cause, surface biofouling, scaling, or deposition of either organic or inorganic foulants into the surface pores.

Combining the effects of both the existence of pores and the losses associated with both viscosity and material damping in the porous structure or frame is needed for a complete model of a porous polymeric membrane. While mathematically quite involved, the models of waves in porous lossy materials are well developed in a general sense [25] as well as for relevant applications [11,26]. The error resulting from the assumptions made in the simpler theory used in much of the literature on membrane ultrasonics can be modest, although variation of theory and

experiment should be interpreted in light of the more complete characterization of the mechanics of waves in a porous material.

2.2. Reflections and transmission at a boundary

While the velocity of the wave is one of the critical parameters for understanding the propagation of the ultrasonic wave, the speed is normally useful primarily in terms of the measured amplitude of the reflection from the membrane. If it is assumed that the signal from the membrane surface can be separated in time from the intervening reflections from the materials used in the membrane module, a classic basic problem from waves in solids is obtained. When an ultrasonic wave is propagated in a fluid that is reflected from the interface with a solid material, the amplitude and refracted angle of the wave in the solid material is a function of the density of the material and the velocity of the wave generated in the solid material. Therefore, we start with a basic configuration for a fully dense material and then will generalize to propagation of the ultrasonic wave in the porous material. The velocity of the wave in a fluid of density ρ_1 is C_1 where only a longitudinal wave is propagated in the fluid.

A solid material of density ρ_2 on which the wave impinges is able to propagate both shear and longitudinal waves in which velocities are a function of the type of wave (shear or longitudinal) and the elastic properties of the medium. In the case considered here of a normally incident longitudinal wave, a shear wave is not generated and the reflection coefficient from the fluid (medium 1) to the membrane (medium 2) takes the simple form of:

$$R_{12}^{A} = \frac{\rho_2 C_2 - \rho_1 C_1}{\rho_2 C_2 + \rho_1 C_1} \tag{13}$$

where ρ_1 is the density of the fluid, C_1 is the velocity in the fluid feed, and ρ_2 is the density of the solid or porous membrane and C_2 is the velocity in the solid or porous membrane. For the transmission coefficient from the fluid into the solid material, the transmission coefficient is:

$$T_{12}^{A} = \frac{2\rho_1 C_1}{\rho_2 C_2 + \rho_1 C_1} \tag{14}$$

which is again simply a function of the product of the density ρ and C, the velocity of the wave of medium 1 (the feed) vs. medium 2 (the membrane). The product of the wave speed and the density is referred to as the acoustic impedance, which is directly analogous to the electrical impedance for a transmission line. It is important to understand, however, that at oblique incidence, the mode conversion into shear waves must be considered, and this simple relation is insufficient for understanding the amplitude of the reflected wave. While the amplitude ratios shown are most clearly defined from a mathematical perspective, it is the acoustic intensity coefficients for transmission and reflection coefficient that are important from the perspective of measurements. From the definition of the acoustic intensity for the problem of normal incidence, $I = A^2/2C\rho$ where A is the amplitude of the wave from Eq. (7). The acoustic intensity reflection coefficient is simply

$$R_{12}^{I} = |R_{12}|^2 \tag{15}$$

Then, the acoustic intensity transmission coefficient is:

$$T_{12}^{I} = \frac{\rho_1 C_1}{\rho_2 C_2} |T_{12}|^2 \tag{16}$$

for which the conservation of energy is satisfied. In the limit where the two materials are the same, the reflection coefficient goes to zero. If the product of the density and the wave speed in the second medium becomes large, then more of the energy is reflected back into the first medium. This effect is evident when looking at the refection from a porous polymeric membrane. In this case, the intensity of the returned acoustic signal is small relative to the incident intensity since the product of the density and wave speed in the membrane is close to the value of water. If this portion of the signal is clearly separated in time from other reflections, then this situation leads to a high level of sensitivity to changes in the interface conditions. However, it also makes these changes vulnerable to interference from other reflecting surfaces, which due to multiple reflections may occur at a similar time. For example, the intensity of the reflection coefficient from the interior of a filament-wound fiberglass pressure vessel would be 5 dB, or at least one order of magnitude greater than the reflection from the interface with the porous polymeric membrane.

While it is beyond the scope of the present discussion, the slow wave will form a separate energy loss which alters the form of Eq. (13). Conceptually, however, the energy is divided into both a slow and fast longitudinal wave in the solid material and thus the reflected energy is reduced when the slow wave is present in the porous material (section 4.3). Because of the number of factors which control the velocity of the

slow wave (Eq. (9)), the form of the relationship is less than straightforward, the physics are similar and the reflection coefficients behave in a manner which is analogous to the behavior of the simpler case presented above [24].

In addition to the basic mechanics of reflection at a solid interface, a number of loss mechanisms exist which can influence the overall amplitude of the signal. In addition to the effect of scattering from suspended solids, which have a smaller effect in most separation processes, salinity, and temperature have a significant but predictable effect on attenuation of the signal [27]. The attenuation as a function of temperature of water and most other fluids is described with a power law where the attenuation α is:

$$\alpha(f) = \alpha_0 f^y \tag{17}$$

where f is the frequency of the wave and the attenuation in water has a value of y which is approximately 2. Additional work has resulted in well-accepted values for ranges of interest in seawater [28]. This effect is in addition to that from scattering and the viscosity, which is reasonably sensitive to the existence of biological materials in the water.

The final aspect of waves in solids which is not considered here are the different types of waves generated due to the existence of boundaries in the direction of propagation of the wave. Waves such as plate waves, which are generated in a thin layer, and surface waves, which are generated on a free surface, may be important for particular applications and have also been considered for manufacturing inspection of porous polymeric membranes [11].

2.3. Generation and analysis of ultrasonic waves

In the previous discussion, it has been assumed that the ultrasonic wave has been generated and propagated though the coupling fluid and that the analysis can be easily performed. However, a number of practical issues exist in this work which should also be considered prior to discussing the application for monitoring of separation processes. For the purposes of this work, it will be assumed that modern commercial piezoelectric transducers will be used along with commercial ultrasonic equipment and high-speed digitization of the received signal. While the details of the design of this instrumentation is beyond the scope of the present work, suffice it to say that the last two decades have seen a transformation of the ability to handle and process the received ultrasonic signals which are generated using the quite mature transducer and analog instrumentation associated with this work.

2.3.1. Piezoelectric transducers

Modern piezoelectric transducers have several critical characteristics which were missing in older instruments. Typically, the elements in these transducers are highly efficient piezoelectric materials such as lead meta-niobates, lead zirconate-lead titanates or lithium niobates, all of which have some temperature sensitivity and can be depoled when used above the allowable temperature range. The manufacturers of the transducers are able to tune the transducers to control the center frequency and bandwidth of the transducer. Broadband transducers for monitoring of separation processes are highly desirable since they result in a pulse which occupies a shorter time window. This allows signals which would otherwise overlap in time to be windowed and allows portions of the signal related to fouling of the membrane to be analyzed without overlap from the larger reflections which are only slightly separated in time. The design of the transducers is such that not only is a short-time signal generated but spurious reflections from the interior of the transducer case which would create problems are eliminated through the design of the transducer housing. It is only with these highly damped broadband transducers that these signals can be effectively analyzed. Use of a large bandwidth transducer also makes it possible to detect the critical frequency transition due to propagation of the slow wave with only a single ultrasonic transducer.

2.3.2. Instrumentation and digitization

While the selection of the transducer is important, excitation of the transducer and digitization of the received signal is required for monitoring of membrane fouling. Most modern ultrasonic systems use either a pulse or a square wave to excite the transducer. By convention, this pulse is a negative voltage which is determined based on the voltage used to pole the piezoelectric ceramics used in the transducers. The combination of a resonant transducer and a broadband electrical excitation allows the pulser to be used for a wide range of frequencies. By substituting a square wave for the pulse excitation, a large increase in the power generated from the transducer can be achieved with only a minimal decrease in the bandwidth of the generated ultrasonic pulse. The analog portion of the instrumentation is then configured in a manner such that either a single transducer can be used to both transmit and receive with a switching system to allow the received signal to be recorded or a separate receiving transducer can be employed. In general, most of the data obtained for fouling of

membranes employed a single ultrasonic transducer that can act as both a transmitter and receiver.

Digitization of the signal is then done in nearly all modern ultrasonic applications. The requirements for the instrumentation are covered in a number of standard references [8]. Among the key requirements for digitizing the signals is that the sampling of the analog signal must be performed at a sufficiently high rate that aliasing of the signal does not occur. The minimum sampling frequency is referred to as the Nyquist frequency, which is the sampling frequency of the signal at a rate that is at least twice the frequency of the highest frequency contained in the signal [29]. This can either be ensured by sampling at a higher rate and filtering or else by making use of an anti-aliasing filter prior to digitization of the signal. For analysis of the signal, the appropriate sampling is critical since the digital processing of the reflected signal is the enabling technology for modern implementation of automated sensing and control. In practice, this is quite simple to achieve with modern instrumentation, since typical bandwidth of an ultrasonic transducer is lower than the sampling rate of most modern oscilloscopes.

2.3.3. General analysis

Once the ultrasonic signal has been digitized, two key elements of the analysis must be addressed. The first element is the existence of dispersion, which is associated with differences in the velocity as a function of frequency. The result can alter the shape of the signal and may result in misinterpretation of the response of the system. The second element is the potential for lack of separation in the signal. The key to design of a monitoring system is to minimize these effects which will result in a simpler and more robust signal processing algorithm.

Dispersion of the signal reflected from the separation interface can result from either the geometry of the structures being investigated or from material damping. The practical result of dispersion is that the simple pulse generated can change shape and be stretched in a manner such that a comparison of the peak amplitude does not give an accurate estimation of the reflection from the separation surface. Similar analysis is required for any ultrasonic signal which interacts with a surface or a body which has any characteristic lengths that are on the same length scale as the wavelength of the ultrasonic wave. For this general and common case, any simple measurements associated with the time signal as display on an oscilloscope or digitized is problematic, since even simple attenuation and velocity measurements need to be done in terms of frequency. However, if we limit this to linear models of the response of the system, a relatively straightforward analysis can be performed using a reference signal from the similar configuration. This reference signal can either be the initial test case for the system prior to fouling or can be a type of reference configuration which will allow all other types of system variation and drift to be accommodated.

In general, the effect of propagation of an ultrasonic signal through a medium cannot be assumed to be independent of frequency. However, if we assume that the system can be reasonably modeled as a linear time-invariant system [8] and if a signal $x(t)$ is propagated through a medium which we designate as S, the resulting system response $y(t)$is the convolution of the input and the system response:

$$y(t) = \int_{-\infty}^{\infty} S(t-\tau)x(\tau)d\tau \tag{18}$$

If the Fourier transform of $y(t)$ is $Y(\omega)$, then in the frequency domain the resulting convolution is:

$$Y(\omega) = S(\omega)X(\omega) \tag{19}$$

where $S(\omega)$ and $X(\omega)$ are the Fourier-transformed response of the medium and the input signal, respectively. This relationship is important since it provides a framework for design of an appropriate reference experiment which can be used in an experimental configuration. The form in which this can be applied is best illustrated with a relevant example.

For the spiral-wound configuration shown in Fig. 3, the signal generated from the ultrasonic transducer, $x(t)$, is convolved with the response from the wall of the pressure vessel, $w(t)$, the transmission coefficient from the wall to the fluid, $T_{wf}(t)$, the response of the fluid surrounding the membrane, $f(t)$, and the reflection from the membrane, $R_m(t)$. The return path results in the response in the opposite direction including the response of the fluid and the pressure vessel wall as well as the transmission coefficient from the fluid to the wall, $T_{fw}(t)$. If the Fourier-transformed response from each of these portions of the signal is considered, then the convolution integrals simply become multiplication in the frequency domain, so that the received signal, $y(t)$ or $Y(\omega)$ in the frequency domain is simply:

$$Y(\omega) = X(\omega)W(\omega)T_{wf}(\omega)F(\omega)R_m(\omega)F(\omega)T_{fw}(\omega)W(\omega) \tag{20}$$

If in turn a well-characterized surface exists in the membrane module such that the reflection coefficient has a known value, this can then serve as the reference experiment. For example, if a surface in the module has the same path as the membrane surface but a reflection coefficient of −1, then for the reference experiment we will have:

$$Y_R(\omega) = X(\omega)W(\omega)T_{wf}(\omega)F(\omega)(-1)F(\omega)T_{fw}(\omega)W(\omega) \quad (21)$$

and then reflection from the membrane will be:

$$R_m(\omega) = \frac{-Y(\omega)}{Y_R(\omega)} \quad (22)$$

While the details of this seemingly simple relationship can be somewhat more complex than the idea, it is in fact a way in which all of the effects such as temperature, pressure, and even the electronic system response can be removed from the analysis. It is also important to note that this analysis either must be performed with a Fourier-transformed signal or else the signal used must contain only a single frequency.

3. Application of ultrasonic measurements to membrane processes

Having reviewed the fundamental physics of ultrasonics in section 2, this section describes the historical development of the use of ultrasonics in membrane applications by noting key contributions to the membrane ultrasonics characterization literature in the areas of membrane structure, compaction, and fouling. Given its importance, the majority of the research has been directed to using the noninvasive, real-time capabilities of ultrasonics for the study of membrane fouling. To provide the reader with an appropriate perspective, recent advances in non ultrasonic approaches to the characterization of membrane fouling are briefly described in section 5.

3.1. Membrane structure

3.1.1. Membrane Formation

Characterization of polymeric membrane formation processes is particularly challenging since the casting solutions are very thin (usually in the range 100–500 μm), and many of their functional properties are typically imparted within seconds. The ability of UTDR to provide high-resolution, nondestructive, real-time characterization is particularly advantageous for this application.

In 1998, Kools et al. [30] published the first application of UTDR to study evaporative casting of cellulose-acetate from an acetone solution containing water as the pore former. Evaporation of the volatile acetone solvent increases the nonsolvent water concentration, thereby eventually causing phase separation. The phase separation front propagates downward through the casting solution, whose thickness simultaneously decreases owing to evaporation and densification. In this study, an ultrasonic transducer was positioned on the underside of the aluminum support plate for the casting solution in order to track both the overall casting solution thickness and the phase-separation boundary. UTDR was able to track locations of two peaks that corresponded to: (1) the upper interface between the phase-separated region and underlying homogenous solution and (2) the liquid–gas interface. The authors observed a progressive decrease in arrival times for both peaks that effectively quantified overall thinning of the casting solution as well as penetration of the phase-separation boundary.

In a recent study by Cai et al. [31], UTDR was used to monitor real-time asymmetric poly(ethylene-co-vinyl alcohol) (EVAL) membrane formation via phase inversion. The objective of the study was to establish a relationship between the phase-inversion rate and the membrane morphology. Membranes were prepared with dimethyl sulfoxide (DMSO) and water (nonsolvent solution). Two 10-MHz ultrasonic transducers were utilized to generate and receive the ultrasonic signals through the casting system. A shift of the ultrasonic signals in the time domain generated by the interface between the bath solution and the casting solution/nascent membrane increased with an increase in membrane formation time. In addition, the shift rate of the ultrasonic signals in the arrival-time domain decreased with an increase in EVAL concentration. Fast diffusion of DMSO into the water bath resulted in the rapid formation of a very thin dense top layer and a sublayer containing macrovoids at a lower EVAL concentration. However, an increase in EVAL concentration led to the formation of finger-like structures owing to a low mass-transfer rate at the higher EVAL concentration. Overall, a meaningful correlation between the ultrasonic measurements and the membrane morphology was established.

As these examples demonstrate, UTDR offers considerable promise for obtaining real-time characterization during membrane formation. Although relatively limited in use to date, the methodology should be capable of providing valuable information during rapid membrane formation processes such as wet-casting process, thermally induced phase separation, and vapor-induced phase separation. Application

to interfacial polymerization (IP) would be quite challenging given that the fully developed IP dense layer is only 100–200 nm thick, a value below the typical resolution limit of arrival-time domain changes. However, the amplitude of the reflected waves might be used to infer the progressive polymerization and cross-linking that occurs during formation.

3.1.2. Membrane morphology

Most commercial membranes are made via continuous casting that involves several processing steps, and quality control ranging from departure from nominal porosity specification to the detection of deleterious defects is important for proper membrane separation performance. The noninvasive and real-time characteristics of UR provide a rationale for its use in membrane quality control, but this application has received relatively limited attention in the literature.

The first attempt to use UR to characterize membrane morphology was reported in the last decade by Gómez Álvarez-Arenas [32]. In this study, a highly sensitive air-coupled piezoelectric transducer was used to relate the ultrasonic attenuation and velocity to the properties of polymeric microfiltration (MF) membranes. However, it was not possible to establish a significant relationship between the ultrasonic measurements and membrane structure, most likely due to the limited resolution of the low-frequency transducers that were employed.

Ramaswamy [33] first applied scanning acoustic microscopy (SAM) to determine the location of pinhole defects with diameters larger than 100 μm inserted into commercial poly(vinylidene) fluoride (PVDF) membranes as well as for identifying partially penetrating defects with diameters ranging from 100 to 300 μm. The presence of macrovoid defects in laboratory-cast cellulose-acetate membranes was also successfully detected. A major advance in membrane morphology characterization was reported by Ramaswamy et al. [34] who utilized UFDR for membrane pore-structure analysis. The goal of this pioneering study was to determine whether UFDR could distinguish pore-size differences in symmetric MF membranes. Commercial PVDF membranes with nominal pore sizes of 0.1, 0.45, and 0.6 μm and mixed cellulose ester membranes (MCE) with nominal pore sizes of 0.1, 0.21, and 0.45 μm were characterized using 90-MHz immersion transducer. The methodology achieved a reasonable compromise between separation of the waveform reflections and adequate sensitivity. Representative results are shown in Fig. 4 where small but significant differences in the frequency-domain

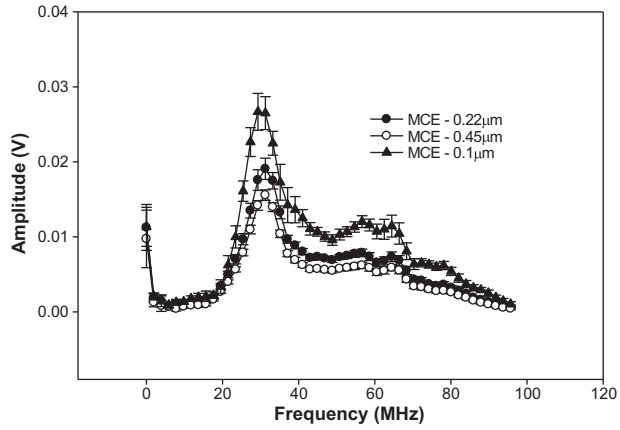

Fig. 4. UFDR spectra from the back-surface reflections of MCE membranes with different nominal pore-size ratings. Decreases in amplitude with increasing pore size are due to more effective scattering by larger pores. Error bars represent variability from five independent membrane samples [32].

spectra for each of the three MCE membranes were attributed to increased scattering with increased membrane mean pore size. These differences were corroborated via scanning electron microscopy (SEM) images and displacement porometry results. The methodology developed incorporated a neural network for differentiating among different membrane morphologies so that the approach could be applied for online noninvasive quality control during membrane manufacturing.

3.2. Membrane compaction

The first publications to describe the application of UTDR for the study of RO membrane compaction were Bond et al. [2], Peterson [35], and Peterson et al. [36]. Membrane compaction, which is more appropriately described as compressive creep, causes an increase in arrival time for the reflection from the membrane surface, since compression moves the membrane-fluid interface away from the transducer. Compaction data are best reported in terms of compressive strain, which is the change in membrane thickness divided by its initial thickness. The common characteristic observed in the aforementioned studies was an inverse relationship between the permeation flow rate (flux) and the compressive strain, i.e. the decrease in the former correlating with the increase in the latter. Of particular importance is that the UTDR work by Peterson et al. [36] documented the decomposition of strain into elastic and inelastic components and indicated that the recovery of these membranes is

time dependent, which possibly explains the hysteresis effects observed when membranes are subjected to pressure cycling. In addition, the authors suggested that the high pressures employed most likely altered either the functional layer (skin) or the interfacial region between the skin and the porous support layer.

A potentially useful application of UTDR is to design membranes that offer improved resistance to compaction. Aerts et al. [37] used UTDR to study the effects of the filler loading on the compaction characteristics of Zirfon asymmetric polysulfone (PS) membranes that were fabricated with a ~0.2-μm dense layer atop a ~340-μm porous substrate, which contained ~0.9-μm zirconia particles. The effect of filler loading on the permeability and compressive strain for pure water permeation were studied. The permeability of the pure PS polymer of this membrane was vanishingly small but increased dramatically with filler content owing to an increase in the porosity of the functional layer. This study clearly demonstrated that UTDR in combination with field-emission scanning electron microscopy (FESEM) can be successfully used to ascertain the effects of filler content on both the functional layer and the substrate. Kelley et al. [38] studied the effects of cross-linking on the compaction resistance of cellulose acetate membranes. These authors used a 4.1 MHz transducer to measure the compressive strain as a function of time for pure water permeation through a cellulose acetate membrane that had been exposed for different periods of time to titanium-isopropoxide cross-linking agent. Their results showed that sufficient cross-linking can reduce the compressive strain by as much as 65% and thus almost completely eliminate the elastic compressive strain.

Although most of the UTDR studies of membrane compaction reported in the literature deal with liquid separations, compaction has also been studied during gas separations. In a pioneering effort, Reinsch et al. [39] described the use of UTDR to measure compaction of asymmetric cellulose acetate gas-separation membranes as a function of feed gas pressure and composition using externally mounted ultrasonic transducers. The authors reported that in nitrogen gas the membranes evidenced an instantaneous strain of ~13% followed by an additional 2% time-dependent strain (Fig. 5). In addition, the study also showed that membrane compaction increases with an increasing concentration of carbon dioxide in the feed stream. The ability to characterize membrane mechanical response to carbon dioxide is of particular interest owing to the plasticizing nature of this gas.

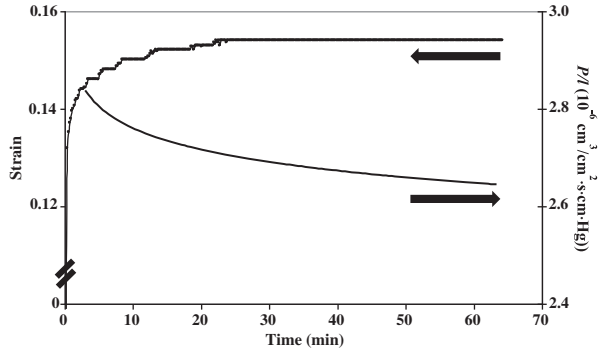

Fig. 5. Representative data for the simultaneous measurement of membrane compaction in nitrogen via UTDR and pressure-normalized flux for a commercial asymmetric cellulose-acetate membrane. The compressive strain response (compaction) consists of elastic and time-dependent components [38].

3.3. Membrane fouling

3.3.1. Inorganic fouling

Inorganic fouling or scaling is a form of fouling that involves the precipitation of sparingly soluble salts, and is well recognized as a major problem in applying membrane technology for high-pressure membrane processes such as the use of RO and NF for desalination. A comprehensive review of scale formation in high-pressure membrane water treatment systems has recently been published by Antony et al. [40]. This paper along with many others confirms the ongoing need for methods for monitoring membrane fouling and cleaning in large-scale water treatment processes as well as to provide fundamental information on the fouling process via bench-scale studies. UR methodology has made an important contribution to these objectives via its documented capabilities for *in situ* nondestructive, real-time characterization of scaling with micron-scale resolution.

The first comprehensive study of membrane fouling using UTDR was that of Mairal et al. [41,42] who studied calcium sulfate dihydrate scaling on a flat-sheet RO membrane in a cross-flow module. Results from Mairal et al. were confirmed by Sanderson et al. [43]. Li et al. [44] used UTDR to study calcium sulfate fouling on flat-sheet RO membranes in both the cross-flow and dead-end modes, and UTDR monitoring of silica fouling on flat-sheet RO membranes was reported by Chong et al. [45]. Zhang et al. [46] and Chai et al. [47] were the first researchers to apply UTDR to monitor calcium sulfate scaling in a commercial 2¼-inch (5.6 cm) spiral-wound RO module, and recently UTDR was employed to characterize calcium sulfate scaling in a commercial 4-inch (10.2 cm)

spiral-wound module [48,49]. UTDR has also been extended to evaluate calcium sulfate scaling for flat-sheet NF membranes [50,51], calcium carbonate scaling [52], synergistic calcium sulfate and microbial fouling on flat-sheet NF membranes [53], kaolin particle fouling on flat-sheet MF membranes [54,55], and fouling on a flat-sheet MF membrane from paper mill effluent [56,57]. In addition, noninvasive monitoring of particle deposition via UTDR was successfully demonstrated for hollow-fiber membranes [58,59], and recently used to monitor fouling by colloidal silica on flat-sheet MF membranes [60]. A new study by Chai et al. [61] builds on prior UTDR studies by utilizing specific waveform peaks to follow a complete cycle of calcium sulfate dihydrate scaling and cleaning in a spiral-wound RO membrane module. In addition, the authors demonstrate the ability of UTDR to distinguish between permeate flux decline owing to scaling and that due to concentration polarization (CP). Results show that amplitude remains constant while permeate flow-rate decreases due to CP caused by addition of soluble sodium chloride (Fig. 6).

Particularly, noteworthy among the aforementioned studies is the development of three complementary ways to analyze the UTDR data. Chai et al. [47] were able to measure the instantaneous local thickness of the scaling deposits by tracking the specific peaks associated with the UTDR reflections from the outmost layers in a spiral-wound module. Zhang et al. [50] developed the concept of the "acoustic signature" characterized by comparing either the arrival time or amplitude of the peaks for the fouled spiral-wound module to those of the same module prior to fouling. Sanderson et al. [57] developed a Fourier wavelet approach whereby the waveform in the time domain is transformed into the frequency domain in order to compare the fouled and unfouled ultrasound response for the same membrane. The ultrasonic signature and Fourier wavelet approaches are advantageous for using UTDR in a control scheme strategy whereby a quantifiable metric is required to determine when some appropriate action should be taken. For example, Lu et al. [62] and Mizrahi et al. [63] recently employed changes in ultrasonic signature to control FR to mitigate scaling in RO desalination (Section 4). These studies indicate that the analysis of specific peaks may be more useful for fundamental studies of membrane fouling where one seeks to determine the nature of fouling at specific locations and times.

3.3.2. Organic fouling

3.3.2.1. Real-time characterization. Organic fouling is a major problem associated with membrane separation processes because it can often severely limit process performance and selectivity [64], and typically occurs either on the external membrane surface leading to cake formation, and/or within the internal membrane structure leading to pore plugging. Organic fouling is a complex phenomenon that depends upon the type of foulant(s), the feed concentration, temperature, pH, and ionic strength, as well as the separation system hydrodynamics. The interplay among these many factors has made a comprehensive understanding of fouling difficult to obtain. There is a significant difference between organic and biological fouling (biofouling). Whereas biofouling is a result of microbial attachment to a membrane and the subsequent growth and release of biopolymers associated with microbial activity, organic fouling is often taken to imply the chemical or physical adsorption of organic compounds to the membrane [65].

Characterization of protein-fouled membranes is crucial to understand fouling mechanisms as well as to minimize fouling maintenance and membrane cleaning cycles [66]. A promising approach for improving the understanding and control of spatially defined fouling mechanisms involves the application of practical models and noninvasive, real-time monitoring, which can be validated using data from actual membrane operations. Clearly, there are significant benefits in employing nondestructive methods that are sensitive only to changes in mass accumulating on a membrane surface or to material that "fills" membrane pores, where these markedly different fouling mechanisms can be isolated from each other. A number of literature studies indicate that UR shows promise in distinguishing between internal pore blockage and surface-cake build-up. Recent reports have described the ability of ultrasonic techniques to monitor the development of organic fouling layers on the surfaces of flat-sheet and hollow-fiber membranes used for drinking water treatment. UTDR has been successfully used to detect protein fouling on tubular ultrafiltration (UF) membranes [67] and organic foulants on hollow-fiber membranes [68,69]. In the study by Li et al. [70], UTDR was used to detect protein on PS UF membranes fouled with a bovine serum albumin (BSA) solution. Results showed good correspondence between the ultrasonic signal responses and the development of BSA association within the membrane microstructure. Sikder et al. [71] used UTDR to monitor the fouling caused by natural brown water from a municipal reservoir, and Silalahi et al. [72] applied UTDR to monitor fouling associated with the use of a flat-sheet MF membrane to separate oil-in-water emulsions.

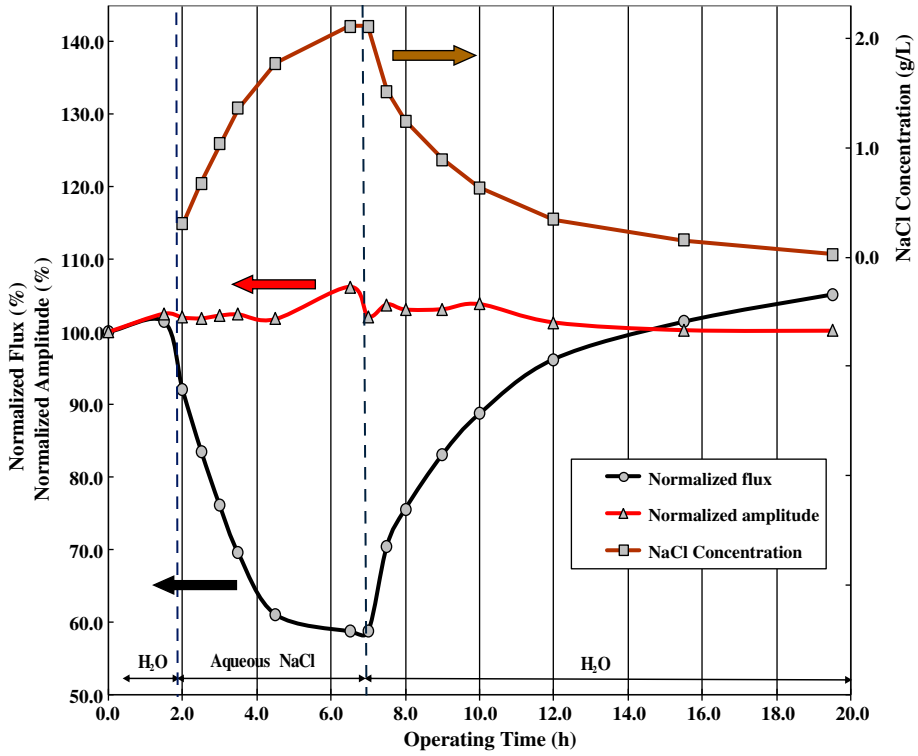

Fig. 6. Normalized permeation flux and normalized UTDR waveform amplitude (left ordinate) and NaCl concentration (right ordinate) as a function of time at a pressure of 0.68 MPa and temperature of 20°C. The feed was DI water until 1.5 h-(vertical dotted line on left), at which time it was switched to a solution of 2.1 g/L of NaCl that caused concentration polarization; at 6.5 h, (vertical dotted line on right) the feed was switched back to DI water that progressively swept out the NaCl. The permeation flux decreases owing to the concentration polarization, whereas the UTDR amplitude remains constant [61].

Kujundzic et al. [73] studied MF membranes challenged with different fractions of industrial fermentation broth and obtained mutually supporting optical, ultrasonic, and hydrodynamic results that suggest that soluble and/or colloidal microbial products associated with planktonic cell growth and not microbial cells themselves, are associated with substantial resistance to transmembrane flow over relatively short periods of time. Importantly, the authors noted that when the module axial dimension is small, the flux and permeate responses occur on the same time scale so that ultrasonic monitoring offers relatively little practical advantage; however, for situations in which the membrane axial dimension is sufficiently large such that organic fouling develops preferentially at one location, ultrasonic methodology would be expected to show a statistically significant departure from baseline values before a corresponding decrease in membrane flux. Such "early warning" of local fouling could be advantageous with respect to optimizing the cleaning of an organic foulant. In addition, Kujundzic et al. [74] explored the ability of UFDR to detect and monitor protein fouling associated with membrane surfaces in flat-sheet cells operating in a laminar cross-flow regime and investigated the use of UFDR to monitor protein fouling in which membrane types, proteins, and protein concentrations are varied. The ultrasonic signal response corresponded well with permeate flow-rate data, and UFDR was able to detect the onset of and continuously monitor protein fouling.

In a recent study by Sim et al. [75], UTDR was adapted to detect biofouling by periodic dosing of colloidal silica as an "acoustic enhancer." This technique was used to detect biofouling on a flat-sheet polyethersulfone (PES) UF membrane and thin-film composite polyamide RO membrane in a "canary cell" configuration. The UTDR response correlated well with post-mortem measurements of biofilm thickness using confocal laser scanning microscopy (CLSM), bacterial counts, and exopolysaccharide (EPS) measurements. Findings showed that colloidal silica does not affect the viability of the bacteria in the biofilm; however, the introduction of colloidal silica can cause an appreciable fouling layer relative to the inherent low hydraulic resistance of the membranes used in low-pressure membrane processes. In contrast,

introducing the colloidal silica appears to have no effect on the transmembrane pressure (TMP) in high-pressure processes such as RO. The researchers concluded that UTDR in combination with silica as an acoustic enhancer could provide an early warning system to measure biofilm growth before increased resistance to permeation caused by biofouling can be observed through a significant change in the TMP profile.

3.3.2.2. Post-mortem characterization. In order to validate UTDR data from real-time membrane performance, a number of standard post-mortem techniques must be used to analyze fouled membranes. Although organics and biofilms have been characterized using various microscopic methods, optical quantification is quite difficult and the degree of accuracy is uncertain. Common means for morphological observation include epifluorescence microscopy (EFM), environmental scanning electron microscopy (ESEM), and CLSM although each of these techniques has associated operating and interpretation obstacles. EFM involves staining microbial cells with fluorescent dyes in which the membrane may interfere with the observations and requires the removal of micro-organisms before their analytical observation. ESEM and CLSM are expensive and labor intensive, and often result in destruction of the biological foulants themselves. Given these limitations, SAM represents a promising tool that can provide an accurate picture of the structure of biological foulants deposited on membrane surfaces.

Confirmation of biofilm occurrence, particularly in the early stages of growth, is critical to the efficient and cost-effective operation of many industrial and medical systems, and may be used to initiate appropriate counter measures to prevent its maturation. Only a limited number of studies have reported results using SAM for the post-mortem characterization of biofouling on polymeric substrates. Kujundzic et al. [76] used UFDR to monitor early-stage biofouling on porous PVDF MF membranes. Membrane coupons were placed in a biologically active annular bioreactor for up to 300 days, and subjected to a constant shear field, which induced sessile microbial growth from acetate-amended municipal tap water. Ultrasonic monitoring was nondestructively performed by traversing coupons in a constant temperature water bath using a spherically focused 20-MHz immersion transducer, and reflections were obtained from 50 regions distributed evenly near the centerline of each coupon. The reflection time and amplitude of reflected sound waves were recorded and compiled into frequency distributions via a Fourier transform. The total reflected power (TRP) from each ultrasonic observation was determined by integrating the amplitude of reflected sound waves through the range of frequency observed. The reflected power distributions were statistically compared with a standard biochemical assay for identifying surface-associated biofilms. Using EPS as a surrogate measure of total biofilm mass, UFDR was able to detect biofilms developing on membrane material tested at surface-averaged masses of $\leq 150\ \mu g/cm^2$. Above these threshold levels, increasing amounts of EPS correlated well with a significant decrease in TRP. When compared to clean conditions, biofilms growing on coupons induced consistent attenuations in reflection amplitude, which caused statistically significant shifts in the reflected power. These results suggest that UFDR may be used as a nondestructive, post-mortem tool to monitor biofouling in a wide variety of applications. SAM has also been used to characterize protein fouling on MF membranes. SAM has also been applied to compare fouling of virgin, broth-fouled, and protein-fouled coupons [73,74]. As expected, post-mortem SAM proved to be more sensitive than real-time ultrasonic monitoring, and showed that ultrasonic spectra from virgin, broth-fouled, and amylase-fouled membrane coupons were statistically different (Fig. 7).

4. Innovative adaptations of UR for membrane fouling measurement

As indicated in section 3, ultrasonic characterization is a well-established technique that has been successfully applied to a wide range of applications. Of these, the use of UR for the detection of fouling has received the most attention given its considerable importance in membrane-based filtration processes. The need to obtain a better understanding of the complex nature of fouling phenomena has driven the continued development of UR. In the following sections, we highlight recent developments that include the use of internal ultrasonic sensors for detection of the onset of inorganic scaling, the first-ever use of ultrasonic sensors as active elements for control of a flow-reversal process for fouling mediation, and the utilization of the so-called slow wave to correlate the deposition of an organic fouling layer with changes in permeability.

4.1. Internal transducers

Previous studies of membrane fouling which employed UR for real-time measurement of inorganic scaling during desalination have all used sensors mounted on the external surface of the module. Recent

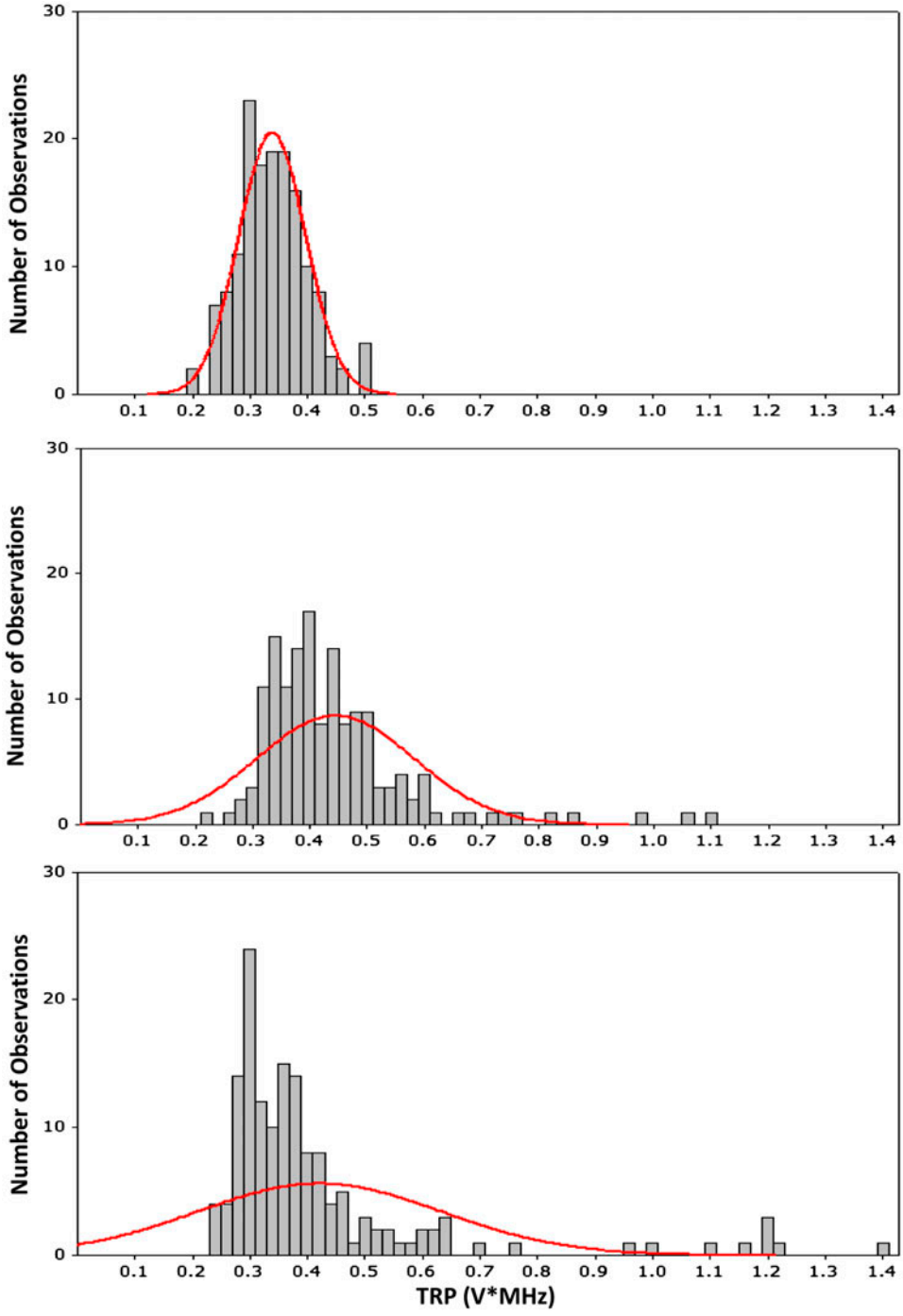

Fig. 7. TRP distributions from MF membrane coupons obtained via SAM. Mean and standard deviation of the distributions in units of V × MHz are given in each figure. TOP: clean; MIDDLE: fouled with broth; and BOTTOM: fouled with amylase. In comparison to the clean coupon, fouling decreases the magnitude and broadens the SAM distribution.

work by Cobry et al. [51] considers the application of miniature-scale ultrasonic transducers that are internally integrated into a flat-sheet cross-flow filtration module such that they are in direct contact with the bottom (back side) of the membrane. The purpose of utilizing this configuration was to determine whether this arrangement would improve the signal sensitivity to obtain better resolution of the onset of scaling. In addition, this study implemented a cross-correlation signal-processing technique to better interpret the

ultrasonic signals regarding the onset of scaling. Moreover, this study utilized a robust statistically based methodology, which has been absent in many previous studies such that conclusions regarding the ultrasonic measurement have been tenuous.

The stainless steel flat-sheet cross-flow cell used in all experiments consisted of a top plate with a recessed cross-flow channel and a bottom plate with a recessed permeate-collection well. The top plate of the cell was placed on the bottom plate, leaving an enclosed flow channel over a NF membrane that was 7.5-cm wide by 55-cm long by 2-mm high, with 4-cm long tapered regions at the two ends to minimize entrance and exit effects. Three delay-line ultrasonic transducers (M203-SM, Olympus) with a center frequency of 10 MHz were mounted internally into the bottom plate of the membrane module as shown in Fig. 8. The delay line on the transducer is also often called a buffer rod, and consists of a cylindrical block of material with low acoustic scattering properties that is mounted to the main transducer face. The opposite face of the delay line is then in contact with the membrane. The delay line separates the echo of interest, i.e. that from the membrane, from the "bang" echo, which always occurs from the primary face of the transducer.

The positioning of the top of the delay line flush with the top of the porous steel support plate and in intimate contact with the underside of the membrane is potentially problematic. The presence of the impermeable surface of the transducer delay line immediately beneath the membrane can impede or totally block permeation through a small area of the membrane (~0.20 cm^2). However, convective mass transfer owing to the cross flow can establish a concentration profile of the calcium sulfate above this small affected area that can cause precipitation of this sparingly soluble salt much in the same way that it occurs in adjacent unimpeded areas of the membrane. The well-conceived experimental design enabled comparisons between signals from the internal transducers and those obtained from externally mounted ultrasonic transducers with a center frequency of 10 MHz (V111, Panametrics) operating simultaneously at corresponding locations.

This study significantly extends the ultrasonic signature approach first proposed by Zhang et al. [46] via a cross-correlation signal-processing technique of the entire ultrasonic waveform with a reference waveform. The reference waveform is from a clean membrane, immediately before the switch from deionized water (DI) feed to salt solution. This procedure is used to obtain a similarity value for the waveforms, to track how they change over time with exposure to the calcium sulfate solution [77]. The signal processing technique accounts for changes in waveform shape over the entire time-domain signal, not just a few selected points. The cross-correlation similarity values were computed and plotted at regular intervals during the experiment. A representative baseline ultrasonic response value is selected shortly before the switch from DI water to calcium sulfate feed; the onset of scaling is determined when the ultrasonic similarity value passes outside of a "breakout threshold" that is chosen to minimize the occurrence of false-positive responses [51].

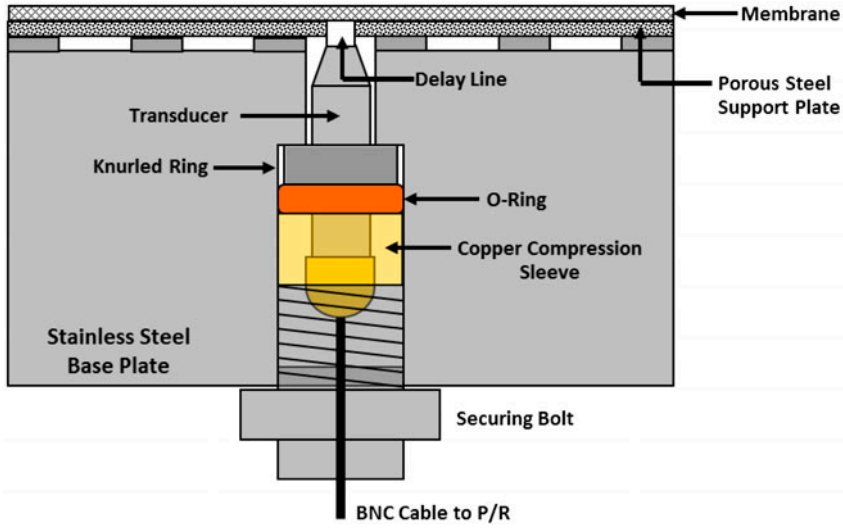

Fig. 8. Schematic showing the integration of an internal ultrasonic sensor with a delay line in a flat-sheet module [51].

The goal of the interval experiments was to correlate responses from the ultrasonic transducers with post-mortem metrics in order to demonstrate a chronological development of early-stage scaling and the ability to detect it. The experiments were performed using an NF membrane (NF-90, Dow FilmTec) under constant operating conditions: pressure of 0.55 ± 0.013 MPa (80 psi), cross-flow velocity of 0.9 cm/s ($Re = 23$), and a feed concentration of 0.47 g/L $CaSO_4$ (0.6 g/L $CaSO_4{\cdot}2H_2O$). These identical experiments were terminated at predetermined times (60, 120, and 150 min) after the switch from DI water to calcium sulfate feed. Fig. 9 shows representative plots of the normalized ultrasonic responses for 60- and 120-min cut-off intervals. The normalized signals through the DI water phase show a relatively constant response with the small variability primarily reflecting the cumulative effect of small changes in operating characteristics. The breakout threshold of 0.4% optimized the accuracy of the scaling signal, i.e. a normalized ultrasonic signal greater than the breakout threshold value. The results indicate that scaling signals were obtained at the downstream location by both internal and external transducers by the end of the 120-min experiments. However, no scaling was ultrasonically detected at the midstream and upstream locations, and no scaling whatsoever was observed at any of the locations for the 60-min experiments. The overall results that include all data from replicate experiments indicate that ultrasonic responses outside the 0.4% breakout threshold were likely to be observed at the downstream location by both internal and external transducers by the end of the 150-min experiments, occasionally by the end of the 120-min experiments and not at all by the end of the 60-min experiments. In summary, these results indicate that the

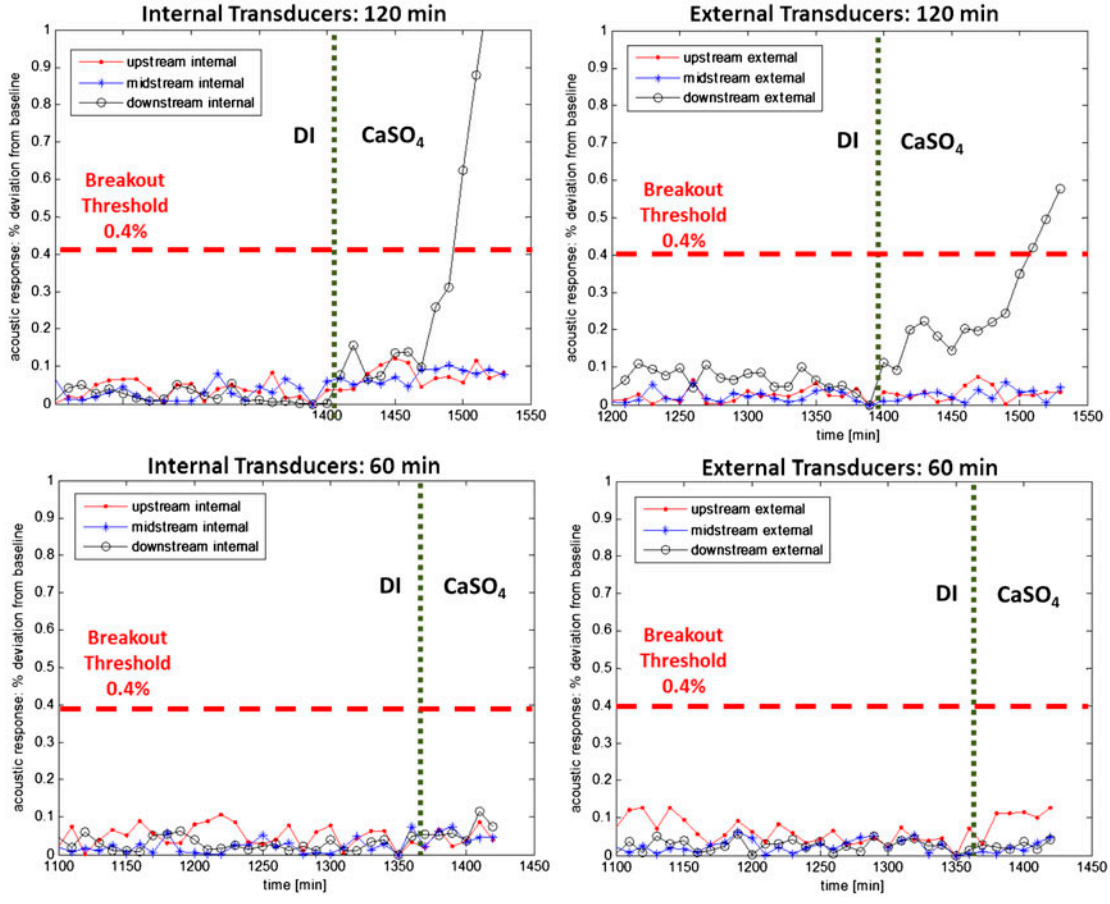

Fig. 9. Representative plots of the normalized cross-correlation ultrasonic responses from the interval experiments where the horizontal dashed line represents a 0.4% breakout threshold and the vertical dotted line indicates the change from DI water to calcium sulfate feed solution. The top row shows the 120-min results for the internal (left) and external (right) transducers and the bottom row shows the 60-min results for the internal (left) and external (right) transducers [51].

ultrasonically determined incubation time for the onset of scaling under these particular operating conditions is between 60 and 120 min.

The area coverage and gravimetric analyses of membrane coupons from time-interval experiments are consistent with the ultrasonic results obtained from the internal and the external sensors, although there is significant variability in the exact magnitude of these values across replicated experiments. Such variability is not unusual for fouling experiments. While no visual or gravimetric evidence of fouling was observed at the upstream or midstream locations, scaling was observed on the downstream internal transducer as well as surrounding areas during both the 120- and 150-min experiments. Representative optical images from membrane coupons at the downstream location after 60-min and 120-min experiments are shown in Fig. 10. These results clearly indicate the lack of scaling at 60 min, but its presence after 120 min. Most importantly, these post-mortem analyses matched the ultrasonic responses shown in Fig. 9. This correspondence confirms that both the external and the internal ultrasonic transducers are capable of detecting the scaling layers. Although the results suggest that the internal transducers can be somewhat more sensitive, the significance of this advantage can be negated by scaling growth that is hindered owing to permeate flow blockage due to the presence of the transducer itself.

Whether an internal or external transducer is utilized, it is important to note that the small sampling area of the transducers may be responsible for false-negatives, i.e. a no-fouling signal when scaling is in fact present. Since both the external as well as the internal ultrasonic transducers essentially provide point measurements, crystal rosette formation might not occur directly in the area sampled ultrasonically. Indeed, given that nucleation sites for calcium sulfate crystal growth are randomly dispersed, the transducer may not sample the presence of an early-stage cluster until it grows to a sufficient size to encroach on the sampling area. This concern could be relatively easily addressed in a larger (pilot-scale) system by increasing the transducer diameter or using an array of transducers to increase the probability of detecting local scale formation.

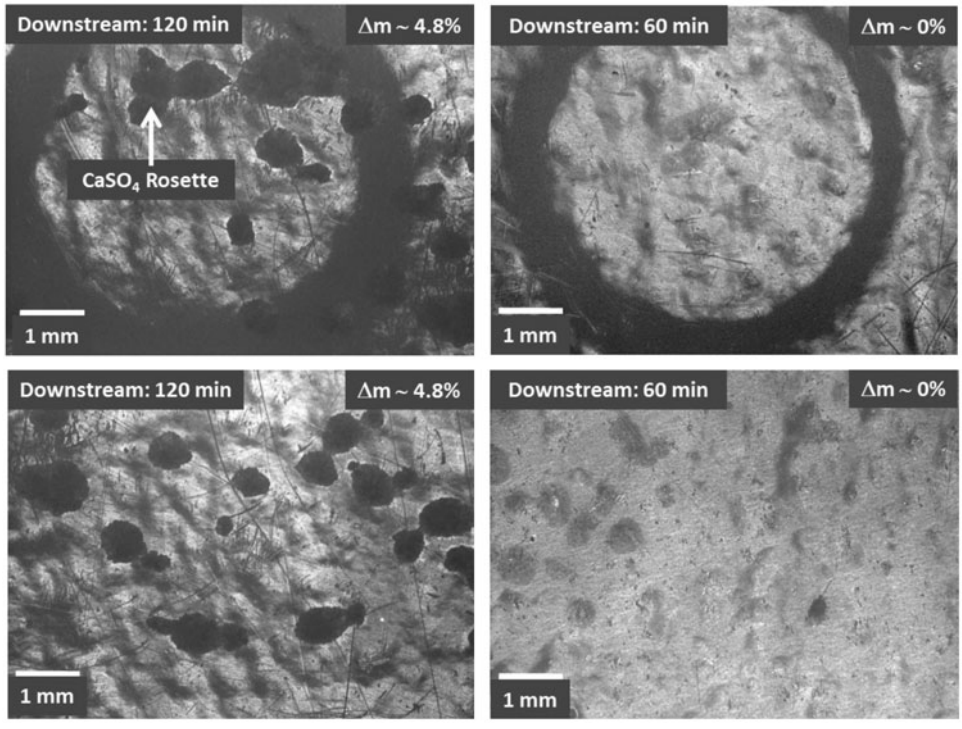

Fig. 10. Light microscopy images of downstream membrane coupon samples from 120-min and 60-min interval experiments that correspond to the ultrasonic results shown in Fig. 9. Scaling (dark regions) is observed after 120 min (left), but the surface remains clean after 60 min (right). Images from the internal transducers areas are shown in the top row (circular imprints) and those from the external transducers are shown in the bottom row (surrounding area, just outside of the circular imprints) [51].

4.2. Ultrasonic sensors as active elements for controlling fouling

A major challenge in utilizing RO desalination is membrane scaling, which is the result of the precipitation of sparingly soluble salts on the surface of the membrane [78,79]. Scaling is of great practical importance since it significantly degrades membrane performance and/or water quality, and hence increases the cost of desalination. Processes to enhance water recovery by adding antiscalants, base softening, or adjusting the pH involve relatively high chemical costs and/or increase the complexity of the overall desalination process [80–82].

During RO, the accumulation of rejected salt ions at the membrane surface results in a higher solute concentration boundary layer at the membrane wall as well as by higher solute concentration at the exit end (downstream) than the entrance end (upstream). The higher concentration encourages surface nucleation and crystal growth (i.e. scaling) at the downstream-end first. This phenomenon underlies the concept of FR in which scaling is mitigated by periodically reversing the flow direction so that the upstream and downstream directions can be switched [83,84]. Recently, FR was linked to induction time, which is the time required for salt nuclei to attain a critical size, above which they continue to grow as scale deposits on the membrane surface [85–87]. A critical issue for the application of FR is the timing of the switch in flow direction. Here, prior knowledge of the induction time or real-time information regarding early-stage scaling is essential. Two recent companion studies by Lu et al. [62] and Mizrahi et al. [63] describe bench-scale experiments which demonstrate that UTDR can provide accurate information about the induction time and enable UTDR-controlled FR to significantly delay the onset of scaling. This work makes the first-ever use of ultrasonic sensors as active elements to automatically control FR.

A sophisticated flat-sheet RO cross-flow cell system was used in which permeate collection is divided into five separate individual sections and corresponding collection ports in order to obtain local permeate flow-rate values at different locations along the flow axis. Three 10-MHz unfocused (flat) ultrasonic transducers (sampling area: 8 mm^2) labeled as A, B, and C are mounted on ports 1, 3, and 5 for monitoring of the *ultrasonic signals* (Fig. 11). A custom LabVIEW program is used to obtain the digitized ultrasonic signals from the three ultrasonic sensors at regular intervals. Two three-way ball valves labeled as V4 and V6 and one two-way by-pass valve labeled as V5 are used so that the system can be operated in forward-flow (FF) and reverse-flow (RF) modes (Fig. 11).

A critical aspect of current experiments involved the use of a novel and powerful algorithm for analyzing the real-time ultrasonic sensor data. The approach employed the concept of a "dynamic amplitude window" in which upper and lower boundaries are established for the average ultrasonic signal amplitude within a particular flow cycle based on the inherent variability of the amplitude under normal nonscaling operating conditions, and these boundaries are adjusted in real time to reflect operating conditions during a particular flow cycle. This adaptive algorithm enables a statistically determined trend line of the average-to-date amplitude vs. time to be established in the absence of an unvarying baseline; when this trend line departs from the amplitude window boundaries, a "breakthrough" is identified and the flow direction in the module is "switched." Breakthrough correlates with end of the induction period and the initiation of local scaling. A number of variations of the dynamic window methodology were considered in order to obtain an optimum balance between sensitivity and "false-positive" responses. A representative result is shown in Fig. 12 where the vertical dashed line indicates the time at which breakthrough occurs. While a dynamic amplitude window and corresponding trend line are obtained from each sensor, the induction time is determined only from the governing sensor, i.e. the downstream sensor (sensor C) in the FF direction and the upstream sensor (sensor A) in the RF direction.

Extensive experiments, each running multiple FF and RF cycles were conducted utilizing feed solutions with different calcium sulfate (RO membrane: FilmTec XLE-440) and calcium carbonate (RO membrane: FilmTec LE-440) concentrations. During the DI water phase for each test, the permeate flow-rate decreased by 20–30% due to membrane compaction. Immediately after the switch from DI water to salt solution, the permeate flow-rate in each port further decreased by approximately 10–30% due to the change of osmotic pressure. The membrane salt rejection calculated based on conductivity measurements of the feed and permeate solutions was 97–99%. During each individual flow cycle, the net permeate flow-rate at each port either decreased due to CP or scaling or increased due to (partial) removal of the scalant. The overall permeate flow-rate, which was defined as the total of the flow rates from three selected ports (1, 3, and 5), is represented in terms of percent decrease by the quantity, SUM.

A series of manually controlled FR experiments was first performed. The permeate flow-rate changes for ports 1, 3, and 5, the overall permeate flow-rate data for a representative test are shown in Fig. 13. The permeate flow-rate values from each port decreased

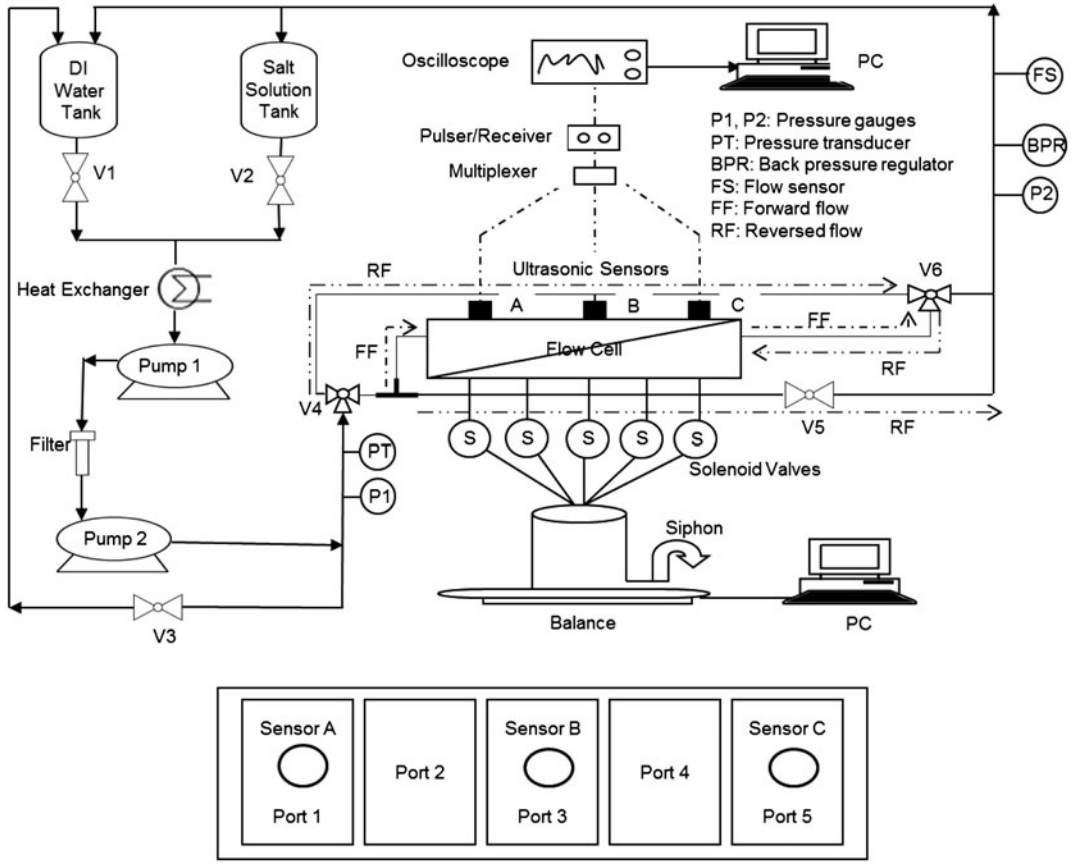

Fig. 11. Top: Schematic showing the bench-scale RO cross-flow system with integrated ultrasonic sensors and instrumentation. Bottom: Top view of the bottom plate of the flat-sheet RO cross-flow cell showing the five permeation ports and the location of three ultrasonic sensors; note that in forward flow, port 1 is upstream and port 5 is downstream, while in reverse flow, port 5 is upstream and port 1 is downstream [62].

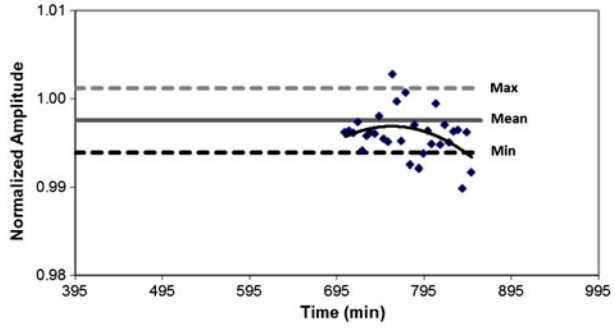

Fig. 12. Representative dynamic amplitude window results for sensor C during a forward-flow cycle. Data obtained over the 395–695-min interval were not included in the calculation of the trend line [62].

immediately after the feed was introduced due to the change in osmotic pressure. After 240 min in the FF1 cycle, a scaling signal was obtained from sensor C, and thus the feed flow direction was switched to RF1. During the RF1 cycle, the permeate flow-rate at port 1 decreased ~11%, while the permeate flow-rate at port 5 fully recovered. After 215 min, a scaling response was obtained from sensor A; so the direction of the flow was changed once again. During the FF2 cycle, the permeate flow-rate at port 1 recovered while the permeate flow-rate at port 5 decreased ~5%. After 65 min, a scaling response was obtained from sensor C so direction of the flow was switched to RF2. During the RF2 cycle, the permeate flow-rate at port 5 increased while that at port 1 decreased. After 35 min, a scaling response was obtained from sensor A, and the test was terminated to confirm the real-time measurements via post-mortem analysis. During this four-cycle test, the net permeate flow-rate decrease in the controlling ports (1 and 5) reached a maximum of 11% whereas the corresponding overall permeate flow-rate decrease was only 2%. This pattern of larger permeate flow decreases in the controlling port, when compared with smaller decreases for the entire membrane, is the desired characteristic for FR.

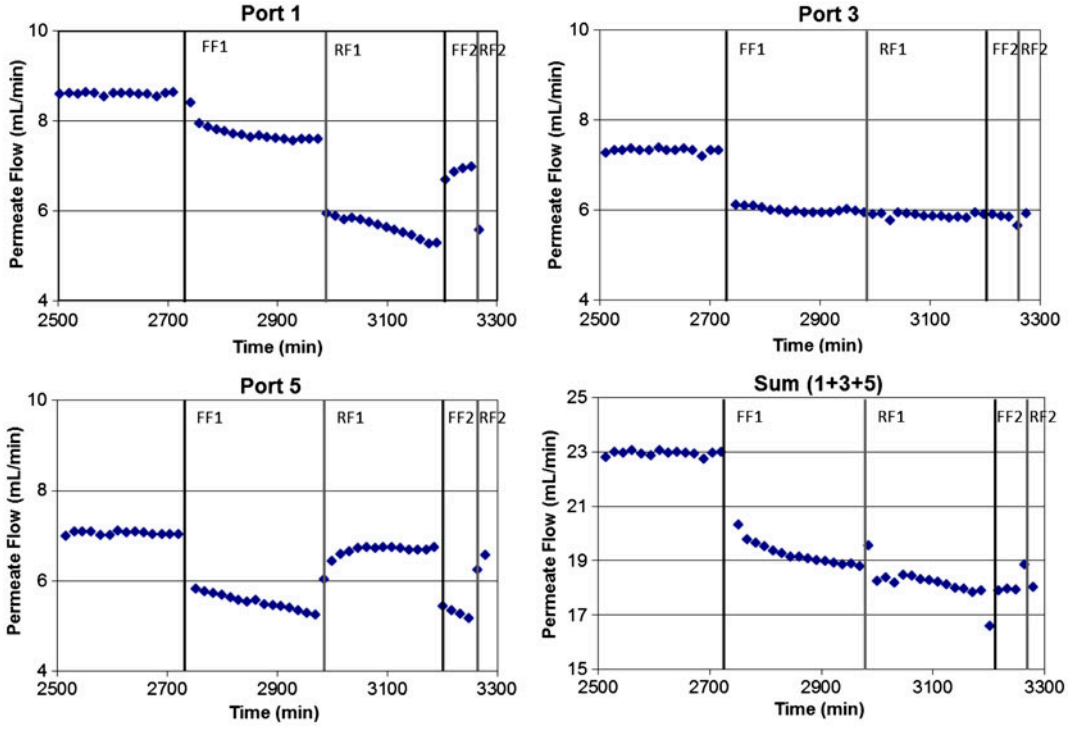

Fig. 13. Absolute permeate flow-rates (mL min^{-1}) for ports 1, 3, and 5 as well as their sum. The interval from 2,500–2,740 min is the end of the DI water phase [62].

The corresponding normalized ultrasonic results for the controlling sensors are shown in Fig. 14. At the completion of the experiment, membrane coupons were cut from the membrane beneath the location of ultrasonic sensors A, B, and C. The post-mortem light microscopy images, gravimetric measurements, and area coverage results are shown in Fig. 15. A mass change of 1% and area coverage of 11% were detected at port 3; these increased to 4 and 19% for mass change, and area coverage, respectively, for port 1 (downstream in the last cycle). Gravimetric measurements and area coverage at port 5 (upstream in the last cycle) were 1 and 9%, respectively, suggesting partial removal of the scaling during this cycle.

With the success of the manual switches, modifications to the flow system enabled automatic switching in response to signals from the ultrasonic sensors. One such experiment was over 75 h in duration and encompassed 19 FF and 19 RF cycles. The permeate flow-rate initially decreased 12, 14, and 14% at ports 1, 3, and 5, respectively, due to osmotic pressure effects. The permeate flow-rate further decreased 8, 4, and 5% at ports 1, 3, and 5, respectively, due to minimal scaling resulting in an overall permeate flow-rate decrease of only 4%. The post-mortem gravimetric and image analysis results showed no scaling at port 1, partial scaling at port 3, and only trace amounts of scaling on the downstream port (port 5). These results were in sharp contrast to an experiment conducted with similar conditions but with no switching for which extensive scaling occurred.

This work documents the first-ever use of UTDR in conjunction with FR for the mitigation of scaling during RO desalination. The ultrasonic sensors successfully distinguished the presence and absence of low levels of scaling in real time on RO membranes operating with FR under realistic conditions. Post-mortem mass and area-coverage characterization data agreed well with real-time ultrasonic and permeate flow-rate behavior. The findings indicate that the methodology successfully responded to early-stage scaling. Most importantly, the work demonstrates the successful adaptation of ultrasonic sensors for active process control. This development represents a significant advance for membrane-based UTDR in comparison to the passive monitoring role that has characterized previous applications. Data from the experiments confirmed that FR, automatically controlled by the sensor hardware/software, can effectively delay scaling and thus mitigate the expected decrease of permeate flow. The success of these current experiments indicated that the methodology

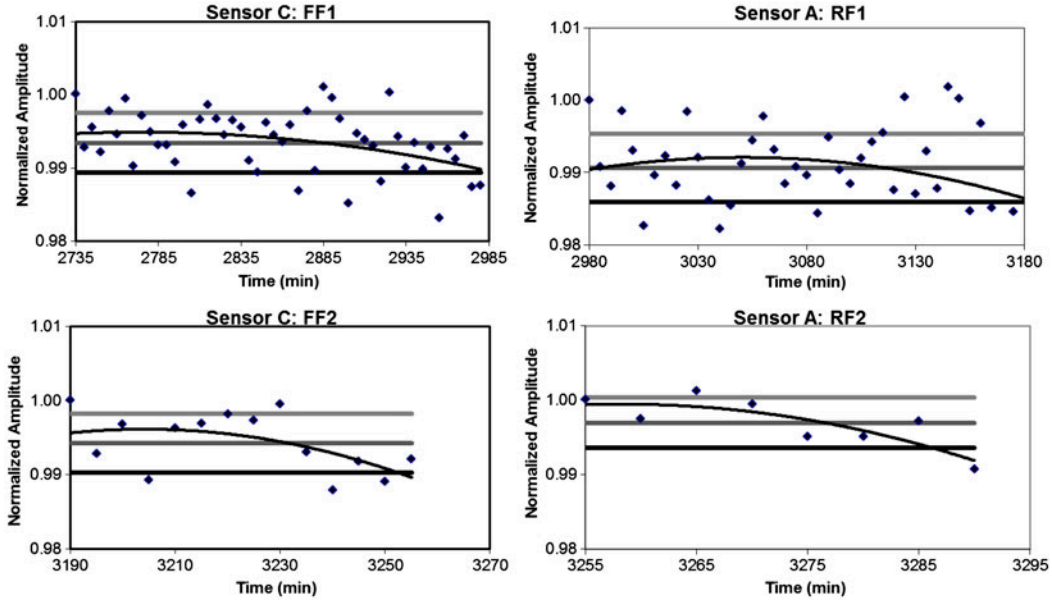

Fig. 14. Dynamic amplitude window results for each cycle from test shown in Fig. 13; Sensor C is controlling sensor during forward-flow and sensor A is the controlling sensor during the reverse-flow cycle. A switch in the flow direction was made when the trend line departed the lower window boundary [62].

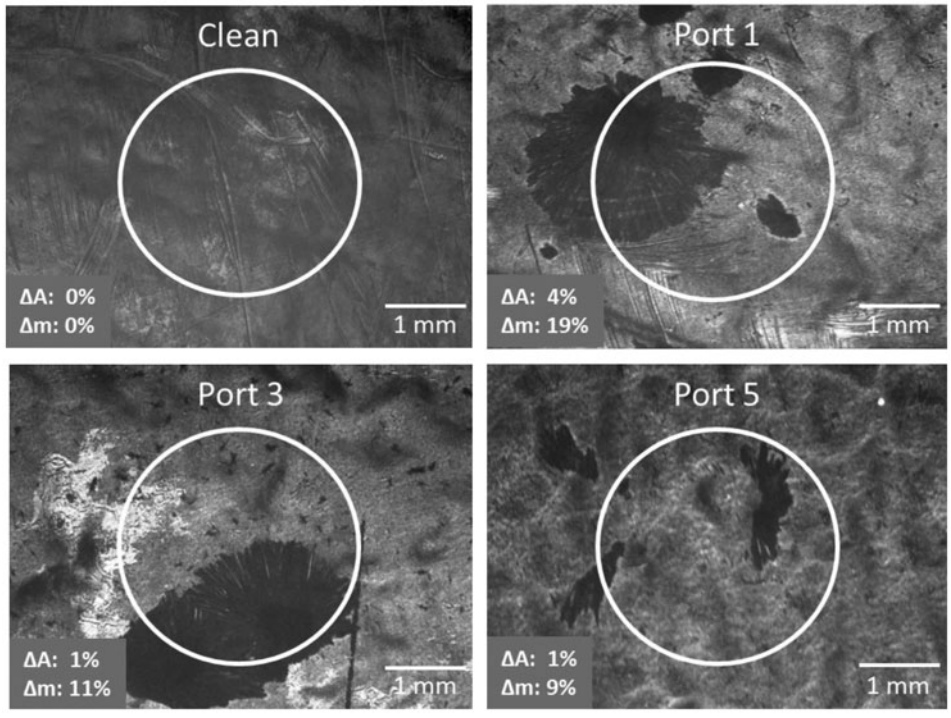

Fig. 15. Post-mortem results for the test shown in Figs. 13 and 14 showing the membrane surface from a clean membrane and those from the three permeation ports. The low-magnification light microscopy images indicate the area coverage (ΔA) of any scaling within the region sampled by the ultrasonic sensor (circle) and the measured mass change (Δm) [62].

was able to accommodate a relatively modest degree of variability in module operating conditions. Confirmation of the effectiveness of ultrasonic sensor-controlled FR in expanded studies would provide a strong basis for using the methodology to facilitate high-recovery RO desalination.

4.3. Slow wave

As indicated in Section 2, monitoring the growth of organic fouling layers formed from proteins or biofilms is more challenging than with inorganic (scaling) layers because the acoustic properties are quite similar to those of the hydrated polymeric membranes on which the fouling occurs. In fact, the organic fouling layers can act as an impedance matching layer between the feed and the hydrated membrane which can reduce the amplitude of the signal reflected from the surface of the membrane, the opposite effect to that seen in scaling. Early-stage growth is particularly difficult to detect using basic ultrasonic techniques. However, since fouling growth typically results in decreasing membrane permeability, an ultrasonic technique which directly measures membrane permeability has the potential to be more reliable and more sensitive than either the basic UTDR and UFDR methods that have been previously employed.

As previously mentioned in section 2.1, Biot [19,20] described the propagation of elastic waves through a fluid-saturated porous medium, and used a semi-phenomenological model to show that three waves exist in a saturated porous material: a fast longitudinal wave, a shear wave, and a slow longitudinal wave. The slow wave is characterized by the out-of-phase movement of the pore fluid and the matrix. This out-of-phase movement of the pore fluid relative to the matrix is very sensitive to the viscosity of the fluid and the permeability of the porous structure. The slow wave has a lower phase velocity and higher attenuation than the fast longitudinal wave [21] with both the phase velocity and attenuation being strongly frequency dependent. This frequency sensitivity provides a unique opportunity to utilize the slow wave to quantify propagation of the slow wave through interconnected pores in a manner consistent with material permeability.

Lin et al. [88] developed an acoustic technique for permeability measurement by measuring the critical wave number of Biot's slow longitudinal wave. The critical wave number can be directly related to the permeability of porous materials. Lin et al. [23,88] also demonstrated experimentally that the critical wave number is associated with a change of permeability caused by either the difference in the pore structure or a change in the viscosity of the pore fluid. These studies suggest that a technique based on the critical wave number measurement may be useful for monitoring the onset of organic layer deposition. Measurement of this change in real time and *in situ* is an essential aspect of this approach since the change in permeability is the critical characteristic of interest, especially for early-stage fouling. In particular, permeability may be decreased by organic layer fouling even though the fouling may not be sufficiently well developed to create a detectable layer on the surface.

A laboratory-scale flow cell was designed with an externally mounted broadband ultrasonic transducer (5-MHz center frequency) and waveguide (Fig. 16). The porous media used in these tests were fabricated by hot-pressing 0.3-μm alumina powder at 1,375 ℃ for 48 min to create samples 46 mm in diameter and 10.5-mm thick with a final density of 1,350 g/cm^3 and a pore volume fraction of 66%. Application of a wet-surface patching epoxy effectively created blockage of the porous ceramic substrate. The epoxy was lightly sanded to ensure that a close-pore condition could be obtained without the formation of an optically detectable layer on the top surface.

Results are summarized in Fig. 17 which shows the measured reflected energy from both open-pore

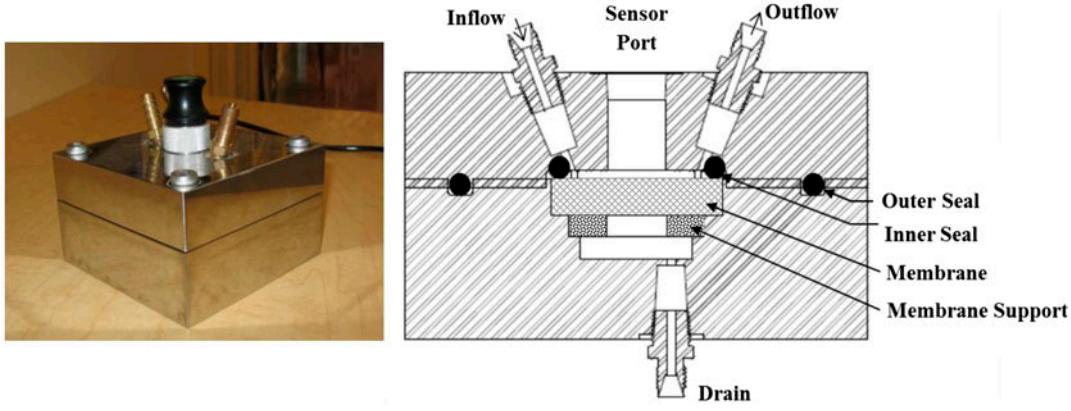

Fig. 16. Left: Photograph of the flow cell with mounted ultrasonic transducer and waveguide; and Right: Schematic of the flow-cell cross-section [89].

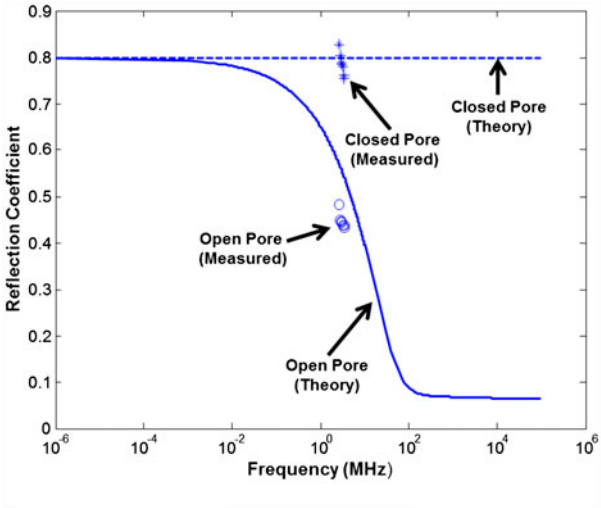

Fig. 17. Reflection coefficient as a function of frequency for the case of the slow wave. Theoretical (lines) and experimental (open circles symbols) results are shown for open-pore and closed pore conditions [89].

and close-pore surfaces as a function of frequency [89]. The data are consistent with theory and indicate that the two measured reflection coefficients are clearly different for the open- and close-pore conditions. Overall, the results indicate that this technique is sensitive to the change of permeability that occurs at the separation membrane surface due to the presence of an organic layer that is sufficiently thin so not to be detectable by other ultrasonic methods. By simply using the reflected signal without understanding the effect of pore closure on the generation of the slow wave, it is not possible to design a robust measurement that is able to detect the presence of a fouling layer.

5. Comparison of UR with other approaches to the measurement of membrane fouling

Given the importance of membrane fouling detection, additional perspective regarding the use of UR can be obtained by considering other approaches to this critical issue. In this section, we first briefly review recent work describing optical methods, impedance spectroscopy, and microsensors, and then consider the major advantages and limitations of UR in comparison.

Several nondestructive methods have been investigated as means for monitoring CP and fouling during membrane-based liquid separations. A good review of *in situ* monitoring techniques is presented by Chen et al. [90]. Despite the abundant theoretical and *ex situ* experimental treatments of CP and fouling, there is still much that is not well understood about these complex and interrelated phenomena [76]. Studies have been performed in which optical methods were used to directly observe CP and fouling. Vilker et al. [91,92] and Ethier and Lin [93] employed similar refractometric techniques by shining collimated light and a laser, respectively, through dead-end filtration cells with high concentration organic solutions (hundreds of g/L). The indexes of refraction of the solutions varied in a known way with concentration such that refraction of the light could be used to describe a concentration profile above the membrane surface. These studies, however, were carried out with very thick CPBL (multiple mm). In a cross-flow configuration, the pressurized feed solution is circulated over the membrane, which reduces osmotic resistance from CP because the rejected component is carried away from the membrane by convective cross flow. This recirculation is not present in dead-end systems, where all of the feed is forced directly through the membrane. Mores and Davis [94] directly observed dyed yeast by mounting a microscope directly above flat-sheet cross-flow modules with transparent top plates.

Optical methods have also been applied in RO flow-reversal systems for timing the switch of the flow direction. As described in section 4.2, prior knowledge of the induction time or real-time information regarding early-stage scaling is essential. Permeate flux decline has been used to monitor early-stage scaling, but this metric normally reflects the average condition of the entire module. Thus, scaling at the downstream end could be significantly advanced by the time that a significant permeate flux decline is detected. To overcome this limitation, an *ex situ* scale observation detector (EXSOD) was designed and integrated into flow-reversal experiments [95]. EXSOD employs real-time digital imaging of the membrane surface to detect the onset of scaling. However, because an optical pathway is required, the EXSOD device is installed in a separate, small RO cell whose input was obtained from the downstream section of the main unit. The ability to accurately detect the onset of scaling in the main unit from measurements made on the bypass module thus depends upon reconciling the different conditions in the two modules.

A related approach to real-time analysis of mineral scale formation on RO membranes was developed by Bartman et al. [96] using an *ex situ* direct observation membrane monitor (MeMo), where the objective of such monitoring is to signal the onset of mineral scaling and provide quantitative information to appropriately initiate system cleaning/scale dissolution. The MeMo used is similar in construction to the EXSOD

previously developed by the same research group. Briefly, the MeMo system consists of a semi-transparent plate-and-frame RO cell that allows for real-time imaging of the surface of a membrane placed in the cell. Mineral scale in the MeMo system is monitored by comparison of consecutive images of the membrane surface to determine the evolution of the fractional coverage by mineral salt crystals and the corresponding crystal count in the monitored region. Through online image analysis, once crystal growth is determined to be above a prescribed threshold, cleaning protocols can be initiated. In addition, MeMo has been evaluated for use in a spiral-wound RO plant in a cyclic mode of feed-FR of brackish water desalting under conditions of high mineral scaling propensity [97]. Scale-free and continuous permeate productivity was demonstrated in an automated spiral-wound RO pilot system in which (calcium sulfate) feed-FR was triggered by scale detection in MeMo.

The influence of a pre-existing biofilm on RO-membrane mineral scaling was evaluated using gypsum as a model scalant in a recent study by Thompson et al. [98]. The biofilm was established using on-site microfiltered secondary-treated wastewater effluent. Mineral scaling was then monitored via direct visual observation of crystal growth on the membrane surface in a transparent plate-and-frame RO cell. Images of the membrane surface were captured at 15-min intervals during each scaling experiment using a high-resolution digital camera that was able to capture six-megapixel images through a set of lenses providing optical magnification. Images were then analyzed to determine the mineral-scaled surface area and crystal count on the membrane surface. The extent of mineral scaling was found to be greater (in terms of both surface scale coverage and crystal number density) in the presence of a biofilm, and was also more pronounced in regions with greater biofilm density.

Impedance spectroscopy has provided a noninvasive means of characterizing the electrical properties of many systems in which important processes occur at the molecular level such as those associated with biological and synthetic membranes and interfaces that form between solutions and various solids (e.g. metals and colloid particles). Coster et al. [99] reviewed the fundamental concepts of impedance spectroscopy and its role in the development of understanding regarding cellular and synthetic membranes, cell biophysics, and ionic systems. Impedance measurements are made by applying a small alternating current of known frequency and small amplitude to a system of interest and measuring the amplitude and phase difference of the concomitant electrical potential. Impedance spectroscopy has been widely used to study membrane structures [100–103] and to investigate membrane fouling and external concentration polarization in pressure-driven membrane processes.

In a recent study by Gao et al. [104], electrochemical impedance spectroscopy (EIS) was applied to a forward osmosis (FO) system to develop a methodology for interpreting the interplay between the membrane structure and the polarization phenomena. The results indicated that EIS appears promising as a means to examine the polarization phenomena during the FO processes. In a recent study [105], real-time EIS measurements were used during the filtration of water containing calcium carbonate constituents in an RO membrane system. Dielectric structural modeling of the EIS measurements was able to detect and characterize five electrically distinct layers and a concentration/diffusion polarization element throughout the filtration experiment. The work indicated that EIS measurements provide a basis for characterizing the structural features of the RO system and monitoring real-time changes that are indicative of scale formation in high-pressure membrane systems.

In the recent years, microsensor technology has been developed for membrane applications. Zhang et al. [50] described a prototype capacitive microsensor for characterizing the vertical profile of the CPBL in calcium sulfate feed solutions in a flat-sheet NF-membrane cross-flow cell. The sensor utilized sets of integrated polysilicon fingers, fabricated on a silicon chip by the Multi-user MEMS Processes (MUMPs). The 2-mm-tall chip was mounted vertically in the module flow channel, and the profile of the cross-flow CPBL was successfully characterized by placing the capacitor sensors at different heights above the membrane surface. However, both of these experiments were conducted under conditions that yielded high concentration and thick boundary layers (several mm), which are not representative of industrial desalination processes.

Recent work by Cobry et al. [106] describes an electrolytic sensor system that can be used in monitoring solute concentration within the thin CPBL that forms near the membrane surface. Experiments were performed in a bench-scale flat-sheet cross-flow system using aqueous calcium sulfate feed solutions. Electronic parameters including capacitance, impedance, phase angle, and conductance were recorded from the sensors, which were also used to detect scaling for which the induction time varied by location (Fig. 18). All of the membrane sensors showed a marked decrease in conductance, which supports the hypothesis that scaling results in a reduction in local

concentration within the CPBL due to precipitation of the supersaturated solute. Additionally, as scaling covers the membrane surface, permeation is locally blocked, which results in a further reduction of CP and the corresponding conductivity. After removal from the module, extensive scaling was observed on the membrane surrounding the downstream sensor, while moderate/light scaling occurred near the upstream sensor, as expected. Although successful, a limitation of the methodology is that the amount of scaling measured by the sensors was less extensive than that on the surrounding membrane, due to local permeation blockage by the sensors. In particular, at low cross-flow velocities, this blockage does have an impact on the local concentration at the immediate sensor location when compared to the surrounding membrane where CP can fully develop.

Clearly, each of these aforementioned techniques has certain advantages as well as limitations in comparison to UR. While each is capable of providing real-time measurement of membrane fouling, some are invasive and thus require modification of the membrane module. In addition, invasive techniques such as direct application of microsensors to the membrane surface can interfere with permeation or can affect local foulant concentrations. Another important aspect of the methodology chosen involves the nature of the data analysis. Whereas application of UR to flat-sheet modules is relatively straightforward with correspondingly simple signal analysis and data reduction, impedance spectroscopy and UR adaptation to a spiral-wound geometry require more complex data analysis for which the robustness of initial assumptions are more critical. Optical methods are limited by the requirement for a suitable transmission pathway and thus the necessity for module modification or the use of a bypass module in which membrane fouling dynamics could be rather different from those in the main module. One important advantage for UR with respect to these other techniques is its relatively low cost. Depending upon the sophistication of the sampling strategy employed, the cost of UR detection using a few directly mounted external transducers, a pulser-receiver, an oscilloscope, and a computer is less than $15,000.

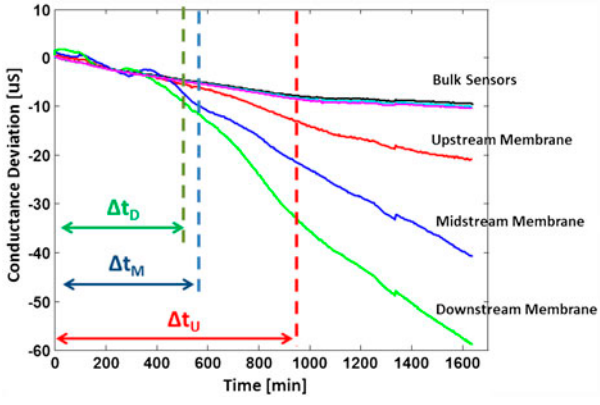

Fig. 18. Conductance data demonstrating scaling formation on the membrane surface where Δt indicates the scaling induction time of each electrolytic membrane sensor, and subscripts labeled as D, M, and U refer to the downstream, midstream, and upstream locations, respectively [106].

6. Summary and future directions

The previous sections of this review have provided reasonably detailed information on ultrasonic fundamentals with particular focus on adaptation to membrane applications, summarized the growing literature on the characterization of membranes and membrane processes via UR, and highlighted particularly innovative aspects of the methodology. In comparison to other techniques, there seems a strong rationale for the wider use of UR given its unique combination of noninvasive, nondestructive, real-time, high spatial, and temporal resolution and low-cost characteristics. Hence, the objective of this section is to suggest valuable future directions for the incorporation of UR in membrane research, development, and practice.

As indicated in the review of the membrane ultrasonics literature in section 3, the principles and instrumentation described in section 2 have been applied to the characterization of membrane structure, compaction, and fouling. As pointed out in Krantz and Greenberg [3], the work of Kools et al. [30] is the first study that makes use of UTDR to characterize membrane-formation processes. In particular, the noninvasive and real-time characteristics in combination with its rapid response enable UTDR to track the relatively rapid densification that occurs during evaporative casting. Given the significant improvement in electronic hardware over the last 15 years, UTDR should be even more amenable to the study of other phase-inversion processes including wet-casting, thermally induced phase separation, and vapor-induced phase separation. Such study could provide important insight into the factors that determine the rate dependence of membrane fabrication and the suitability of modeling efforts to represent the phase transformations that ultimately govern final structure. In many ways, the adaptation of UR for defect detection and pore-size comparison as described in Ramaswamy et al. [33,34] is less demanding than its use in the aforementioned membrane formation studies. Thus, the potential for employing UR for online quality control of membrane fabrication remains as a productive area for further development.

It is well recognized that membrane compaction, i.e. creep, can affect membrane performance, most often via decreased permeate flux. Quantification of real-time compaction behavior using UR has been documented by Peterson et al. [35,36] for liquid separations and Reinsch et al. [39] for gas separation. Compaction properties depend on the physical and chemical structure of the membrane as well as the operating conditions. Work by Aerts et al. [37] and Kelly et al. [38] showed that UR was quite effective in measuring changes in the compaction response as a result of filler addition and crosslinking. There is room for improvement in this application for UR because of the complications that arise from asymmetric structures in which a "skin," a porous supporting layer, and a nonwoven layer on which the membrane is casted have significantly different thicknesses and can evidence creep to varying degrees. Improved resolution would enable determination of these differential responses rather than a "pooled" response for the membrane as a whole. In addition, establishing more accurate creep data for component layers would enable more effective studies relating creep to specific structural changes such as pore size as well as providing a firmer basis for developing membranes with improved performance characteristics. Finally, it is worth noting the almost complete lack in the literature of quantitative information regarding the effect of temperature and pressure on membrane compaction. This could easily be addressed by the use of UR to systematically assemble a suitable database.

While the aforementioned application areas are clearly amenable to further study, it is in the area of membrane fouling and cleaning where the use of UR may ultimately generate the most impact. In addition to the many prior studies of membrane fouling employing this technique noted in section 3, the recent research highlighted in section 4, which utilizes particularly innovative approaches for the use of UR in the critical area of membrane fouling, provides useful insight regarding the unrealized potential of the methodology.

The work by Lu et al. [62] and Mizrahi et al. [63], documents the first-ever use of UTDR in conjunction with FR for the mitigation of scaling during RO desalination. The work utilized a downstream and an upstream ultrasonic sensor corresponding to feed flow in the forward and reverse direction, respectively, and involved the development of a novel algorithm for analyzing the real-time ultrasonic sensor data such that the departure of a trend line constituted a scaling signal that mandates a change in the flow direction. The ultrasonic sensors successfully distinguished the presence and absence of low levels of scaling in real time on RO membranes operating with FR under realistic conditions. Most importantly, the work demonstrates the successful adaptation of ultrasonic sensors for active process control. This development represents a significant advance for membrane-based UTDR in comparison to the passive monitoring role that has characterized previous applications. Data from the experiments confirmed that FR automatically controlled by the sensor hardware/software can effectively delay scaling and thus mitigate the expected decrease of permeate flow. The success of these current experiments indicated that the methodology was able to accommodate a relatively modest degree of variability in module operating conditions. Nonetheless, additional testing is required under a broader range of operating parameters and feed compositions. Confirmation of the effectiveness of ultrasonic sensor-controlled FR in such expanded studies would provide a strong basis for using the methodology to facilitate high-recovery RO desalination. Technology could involve either direct monitoring of spiral-wound modules or indirect approach using a flat-sheet module in conjunction with a bypass stream.

Whereas the use of UR for the measurement of organic fouling has been modestly successful in real-time experiments, direct *in situ* detection of early-stage biofilm deposition under realistic operating conditions is still problematic. Such detection is quite challenging for a number of reason including the tendency for such layers to evidence significant temporal and spatial variability. In addition, the problem is made more complex since biofilm formation often occurs simultaneously with other types of fouling. Indeed, the challenge of detecting fouling from complex feeds is a major concern in its own right. Given the importance of early-stage biofilm detection, other approaches are needed to overcome the current ultrasonic detection limitations. Here, the work of Lin et al. [23] described in section 4 provides an intriguing possibility in that early-stage biofilm fouling might be inferred from the ultrasonic detection of permeability changes. For now, this idea remains undeveloped since Lin et al. [23] employed a pre-applied, uniform layer of epoxy rather than a variable biofilm for their experiments. Nonetheless, the prospect of relating local surface characteristics and flow behavior via ultrasonic measurements deserves further study.

Clearly, a critical next step for application of UR is to combine the important insights from prior work in detecting scaling onset and removal in spiral-wound modules during NF and RO desalination with the innovative approaches described in sections 4.1 and 4.2 that incorporate hardware and software development. As well documented in the literature, there are

significant technical challenges in adapting UR to spiral-wound modules including the complex multiple material, multilayer geometry, high-attenuation characteristics of the shell and filter wrapping, and the effects of changes in the operating parameters on the ultrasonic signal characteristics. Indeed, recent work by Chai et al. [61] confirms that changes in temperature and pressure must be taken into account to provide accurate information regarding membrane scaling in spiral-wound modules. However, the relatively limited findings of this study indicate that a more comprehensive and systemic evaluation of temperature and pressure effects on ultrasonic characteristics in a variety of different spiral-wound modules is warranted. When such information is combined with improved signal-analysis software, more accurate and useful information can be obtained from the complex ultrasonic spectra. Indeed, while prior studies have confirmed that UR can provide noninvasive, real-time detection of membrane fouling and cleaning, important issues must be addressed before the methodology can be routinely applied to membrane desalination on a commercial scale. There is a compelling rationale for doing so given an expectation of a rapid increase in the size of the desalination market in 2013 led by more than $5 billion annual investment by Saudi Arabia and followed by an expected investment of nearly $4.5 billion by the United States [107].

In summary, we reiterate the recommendations of the prior review [3], and note the importance of industry participation in the exploration and development of UR applications for large-scale membrane modules and processes. Hence, we emphasize the need for cooperative efforts between industry and university research institutions to utilize the full capabilities of UR.

Abbreviations

$CaSO_4$ — calcium sulfate
CLSM — confocal laser scanning microscopy
CP — concentration polarization
CPBL — concentration polarization boundary layer
DI — deionized
DMSO — dimethyl sulfoxide
ECP — external concentration polarization
EFM — epifluorescence microscopy
EIS — external impedance spectroscopy
EPS — exopolysaccharide
ESEM — environmental scanning electron microscopy
EVAL — poly(ethylene-co-vinyl alcohol)
EXSOD — *ex situ* scale observation detector
FESEM — field emission scanning electron microscopy
FF — forward flow
FO — forward osmosis
FR — flow reversal
IP — interfacial polymerization
MCE — mixed cellulose ester
MeMo — *ex situ* scale observation detector membrane monitor
MF — microfiltration
MUMPs — multi-user micro-electromechanical systems (MEMS) processes
NaCl — sodium chloride
NF — nanofiltration
PES — polyethersulfone
PS — polysulfone
PVDF — poly(vinylidene fluoride)
Re — Reynolds number
RF — reverse flow
RO — reverse osmosis
SAM — scanning acoustic microscopy
SEM — scanning electron microscopy
TMP — transmembrane pressure
TRP — total reflected power
UF — ultrafiltration
UR — ultrasonic reflectometry
UFDR — ultrasonic frequency-domain reflectometry
UTDR — ultrasonic time-domain reflectometry

Symbols

ΔA — change in area coverage (%)
A — amplitude (V)
B — bulk modulus (GPa)
C — velocity of the acoustic wave (km/s)
E — Young's modulus (GPa)
f — frequency (Hz)
I — normal incidence
k_{cr} — critical wave number for the slow wave (radians/m)
Δm — change in mass (%)
p — pressure (kPa)
R_{ab} — reflection coefficient in medium 1 from medium 2
s — salinity (ppt)
T — temperature (°C)
T_{ab} — transmission coefficient from medium 1 to 2
t — time (μsec)
Δt — scaling induction time (min)
u — displacement (μm)

Greek

α — attenuation (Nepers/m)
n_0 — porosity (%)
λ' — Lame's elastic constant (GPa)
λ — wavelength (nm)
μ — shear modulus (GPa)
ν — Poisson's ratio
ρ — density (kg/m^3)
υ_f — fluid viscosity (MPa·s)
ϕ — Darcy is a unit for permeability of the porous solid
ω — angular frequency (rad/s)

Acknowledgment

The authors thank all of those who have contributed over the years to the growing body of work that involves the use of ultrasonics for membrane applications. We are pleased to acknowledge that many of these applications were initiated and supported by the NSF Industry/University Cooperative Research Center for Membrane Science, Engineering and Technology Center at the University of Colorado-Boulder (IIP 1034720) and its predecessors.

References

[1] G. Hoest, J. Brewster, A.R. Greenberg, L. Bond, W.B. Krantz, Real-time noninvasive measurement of membrane compaction and fouling, 6th Annual Meeting of the North American Membrane Society, Breckenridge, CO, 1994.
[2] L.J. Bond, A.R Greenberg, A.P. Mairal, G. Loest, J.H. Brewster, W.B. Krantz, in: D.O. Thompson, D.E. Chimenti (Eds.), Review of Progress in Quantitative Nondestructive Evaluation, Plenum Press, New York, NY, 1995, pp. 1167–1173.
[3] W.B. Krantz, A.R. Greenberg, Membrane characterization by ultrasonic time-domain refelectometry, in: A.G.F. N.N. Lee, W.S.W. Ho, T. Matsura (Eds.), Advance Membrane Technology and Applications, Wiley, 2008, pp. 879–897.
[4] A.D. Pierce, Acoustics: An Introduction to Its Physical Principles and Applications, Acoustical Society of America, New York, NY, 1989.
[5] P.M. Morse, K.U. Ingard, Theoretical Acoustics, Princeton University Press, Princeton, NJ, 1987.
[6] J.D. Achenbach, Wave propagation in elastic solids, in: H.A. Lauwerier, W.T. Koiter (Eds.), Applied Mathematics and Mechanics, North-Holland Publishers, Amsterdam, Netherlands,1987.
[7] K.A. Graff, Wave Motion in Elastic Solids, Dover Publications, Mineola, New York NY, 1991.
[8] L.W.J. Schmerr, Fundamentals of Ultrasonic Nondestructive Evaluation, Springer, 1998.
[9] S.B. Barnett, G.R. Ter Haar, M.C. Ziskin, H.D. Rott, F.A. Duck, K. Maeda, International recommendations and guidelines for the safe use of diagnostic ultrasound in medicine, Ultrasound Med. Biol. 26 (2000) 355–366.
[10] T. Bourbie, O. Coussy, B. Zinszner, Acoustics in Porous Media, Technip, Paris, 1987.
[11] M.L. Peterson, A. DiLeo, Z.M. Wang, A. Greenberg, Ultrasonic Detection of Porous Medium Characteristics, US Patent number: 6959602, Filing date: March 12 2003, issued November 1, 2005.
[12] L. Lin, M.L. Peterson, A.R. Greenberg, Generation and propagation of ultrasonic plate wave in fluid-loaded porous polymeric membrane, Insight 49 (2007) 213–216.
[13] V.K. Kinra, V.R. Iyer, Ultrasonic measurement of the thickness, phase velocity, density or attenuation of a thin-viscoelastic plate, Part I: The forward problem, Ultrasonics 33 (1995) 95–109.
[14] V.K. Kinra, V.R. Iyer, Ultrasonic measurement of the thickness, phase velocity, density or attenuation of a thin-viscoelastic plate, Part II: The inverse problem, Ultrasonics 33 (1995) 111–122.
[15] R. Demirli, J. Saniie, Model-based estimation of ultrasonic echoes, Part II: Nondestructive evaluation applications, IEEE Trans. Ultrason. Ferroelectr. Freq. Control 48 (2001) 803–811.
[16] A.I. Lavrentyev, S.I. Rokhlin, Determination of elastic moduli, density, attenuation, and thickness of a layer using ultrasonic spectroscopy at two angles, J. Acoust. Soc. Am. 102 (1997) 3467–3477.
[17] Y.C. Fung, Foundations of Solid Mechanics, Prentice Hall, Englewood Cliffs, NJ, 1965.
[18] O. Dazel, V. Tournat, Nonlinear Biot waves in porous media with application to unconsolidated granular media, J. Acoust. Soc. Am. 127 (2010) 692–702.
[19] M.A. Biot, Theory of propagation of elastic waves in a fluid-saturated porous solid. I. Low-frequency range, J. Acoust. Soc. Am. 28 (1956) 168–178.
[20] M.A. Biot, Theory of propagation of elastic waves in a fluid-saturated porous solid. II. Higher frequency range, J. Acoust. Soc. Am. 28 (1956) 179–191.
[21] T.J. Plona, Observation of a second bulk compressional wave in a porous medium at ultrasonic frequencies, Appl. Phys. Lett. 36 (1980) 259–261.
[22] I. Edelman, Bifurcation of the Biot slow wave in a porous medium, J. Acoust. Soc. Am. 114 (2003) 90–97.
[23] L. Lin, M.L. Peterson, A.R. Greenberg, B.A. McCool, In situ measurement of permeability, J. Acoust. Soc. Am. 125 (2009) El123–El128.
[24] K.Y. Wu, Q. Xue, L. Adler, Reflection and transmission of elastic waves from a fluid-saturated porous solid boundary, J. Acoust. Soc. Am. 87 (1990) 2349–2358.
[25] M.A. Biot, Generalized theory of acoustic propagation in porous dissipative media, J. Acoust. Soc. Am. 34 (1962) 1254–1254.
[26] P. Goransson, Acoustic and vibrational damping in porous solids, Philos. Trans. Roy. Soc. A 364 (2006) 89–108.
[27] S.D. Richards, The effect of temperature, pressure, and salinity on sound attenuation in turbid seawater, J. Acoust. Soc. Am. 103 (1998) 205–211.
[28] F.H. Fisher, V.P. Simmons, Sound absorption in sea water, J. Acoust. Soc. Am. 62 (1977) 558–564.
[29] A.V. Oppenheim, R.W. Schafer, J.R. Buck, Discrete-Time Signal Processing, Prentice Hall, Upper Saddle River, NJ, 1999.
[30] W.F.C. Kools, S. Konagurthu, A.R. Greenberg, L.J. Bond, W.B. Krantz, T.Van Den Boomgaard, H. Strathmann, Use of ultrasonic time-domain reflectometry for real-time measurement of thickness changes during evaporative casting of polymeric films, J. Appl. Polym. Sci. 69 (1998) 2013–2019.
[31] Y. Cai, J.X. Li, Y.G. Guo, Z.Y. Cui, Y.Z. Zhang, In-situ monitoring of asymmetric poly(ethylene-co-vinyl alcohol) membrane formation via a phase inversion process by an ultrasonic through-transmission technique, Desalination 283 (2011) 25–30.
[32] T.E. Gómez Álvarez-Arenas, Air-coupled ultrasonic spectroscopy for the study of membrane filters, J. Membr. Sci. 213 (2003) 195–207.

[33] S. Ramaswamy, Development of an Ultrasonic Technique for Non-invasive Characterization of Membrane Morphology, PhD Thesis, Department of Chemical Engineering, University of Colorado, Boulder, 2002.
[34] S. Ramaswamy, A.R. Greenberg, M.L. Peterson, Non-invasive measurement of membrane morphology via UFDR: Pore-size characterization, J. Membr. Sci. 239 (2004) 143–154.
[35] R.A. Peterson, Use of acoustic TDR to assess the effect of crosslinking on membrane compaction, Department of Mechanical Engineering, University of Colorado at Boulder, Boulder, 1996.
[36] R.A. Peterson, A.R. Greenberg, L.J. Bond, W.B. Krantz, Use of ultrasonic TDR for real-time noninvasive measurement of compressive strain during membrane compaction, Desalination 116 (1998) 115–122.
[37] P. Aerts, A.R. Greenberg, R. Leysen, W.B. Krantz, V.E. Reinsch, P.A. Jacobs, The influence of filler concentration on the compaction and filtration properties of Zirfon-composite ultrafiltration membranes, Sep. Purif. Technol. 22–23 (2001) 663–669.
[38] S.S. Kelley, J. Filley, A.R. Greenberg, R. Peterson, W.B. Krantz, Chemical modification of cellulose acetate with titanium isopropoxide, Int. J. Polym. Anal. Charact. 7 (2002) 162–180.
[39] V.E. Reinsch, A.R. Greenberg, S.S. Kelley, R. Peterson, L.J. Bond, A new technique for the simultaneous, real-time measurement of membrane compaction and performance during exposure to high-pressure gas, J. Membr. Sci. 171 (2000) 217–228.
[40] A. Antony, J.H. Low, S. Gray, A.E. Childress, P. Le-Clech, G. Leslie, Scale formation and control in high pressure membrane water treatment systems: A review, J. Membr. Sci. 383 (2011) 1–16.
[41] A.P. Mairal, A.R. Greenberg, W.B. Krantz, L.J. Bond, Real-time measurement of inorganic fouling of RO desalination membranes using ultrasonic time-domain reflectometry, J. Membr. Sci. 159 (1999) 185–196.
[42] A.P. Mairal, A.R. Greenberg, W.B. Krantz, Investigation of membrane fouling and cleaning using ultrasonic time-domain reflectometry, Desalination 130 (2000) 45–60.
[43] R.D. Sanderson, J.X. Li, L.J. Koen, L. Lorenzen, Ultrasonic time-domain reflectometry as a non-destructive instrumental visualization technique to monitor inorganic fouling and cleaning on reverse osmosis membranes, J. Membr. Sci. 207 (2002) 105–117.
[44] J.X. Li, L.J. Koen, D.K. Hallbauer, L. Lorenzen, R.D. Sanderson, Interpretation of calcium sulfate deposition on reverse osmosis membranes using ultrasonic measurements and a simplified model, Desalination 186 (2005) 227–241.
[45] T.H. Chong, F.S. Wong, A.G. Fane, Fouling in reverse osmosis: Detection by non-invasive techniques, Desalination 204 (2007) 148–154.
[46] Z.-X. Zhang, A.R. Greenberg, W.B. Krantz, G.-Y. Chai, Study of membrane fouling and cleaning in spiral wound modules using ultrasonic time-domain reflectometry, in: D. Bhattacharyya (Ed.), New Insights into Membrane Science and Technology: Polymeric, Inorganic and Biofunctional Membranes, Vol. 8, Elsevier, Amsterdam, 2003, pp. 65–88.
[47] G.Y. Chai, A.R. Greenberg, W.B. Krantz, Ultrasound, gravimetric, and SEM studies of inorganic fouling in spiral-wound membrane modules, Desalination 208 (2007) 277–293.
[48] G.H. An, J.B. Lin, J.X. Li, X.Q. Jian, In situ monitoring of membrane fouling in spiral-wound RO modules by UTDR with a sound intensity modeling, Desalin. Water Treat. 32 (2011) 226–233.
[49] G.H. An, J.B. Lin, J.X. Li, X.H. Li, X.Q. Jian, Non-invasive measurement of membrane scaling and cleaning in spiral-wound reverse osmosis modules by ultrasonic time-domain reflectometry with sound intensity calculation, Desalination 283 (2011) 3–9.
[50] Z.X. Zhang, V.M. Bright, A.R. Greenberg, Use of capacitive microsensors and ultrasonic time-domain reflectometry for in-situ quantification of concentration polarization and membrane fouling in pressure-driven membrane filtration, Sensor Actuat. B-Chem. 117 (2006) 323–331.
[51] K.D. Cobry, Z. Yuan, J. Gilron, V.M. Bright, W.B. Krantz, A.R. Greenberg, Comprehensive experimental studies of early-stage membrane scaling during nanofiltration, Desalination 283 (2011) 40–51.
[52] J. Li, J. Liu, T. Yang, C. Xiao, Quantitative study of the effect of electromagnetic field on scale deposition on nanofiltration membranes via UTDR, Water Res. 41 (2007) 4595–4610.
[53] Y.L. Hou, Y.A. Gao, Y. Cai, X.C. Xu, J.X. Li, In-situ monitoring of inorganic and microbial synergistic fouling during nanofiltration by UTDR, Desalin. Water Treat. 11 (2009) 15–22.
[54] J.X. Li, R.D. Sanderson, E.P. Jacobs, Non-invasive visualization of the fouling of microfiltration membranes by ultrasonic time-domain reflectometry, J. Membr. Sci. 201 (2002) 17–29.
[55] J.X. Li, R.D. Sanderson, In situ measurement of particle deposition and its removal in microfiltration by ultrasonic time-domain reflectometry, Desalination 146 (2002) 169–175.
[56] J.X. Li, D.K. Hallbauer, R.D. Sanderson, Direct monitoring of membrane fouling and cleaning during ultrafiltration using a non-invasive ultrasonic technique, J. Membr. Sci. 215 (2003) 33–52.
[57] R.D. Sanderson, J.X. Li, D.K. Hallbauer, S.K. Sikder, Fourier wavelets from ultrasonic spectra: A new approach for detecting the onset of fouling during microfiltration of paper mill effluent, Environ. Sci. Technol. 39 (2005) 7299–7305.
[58] X.C. Xu, J.X. Li, H.S. Li, Y. Cai, Y.H. Cao, B.Q. He, Y.Z. Zhang, Non-invasive monitoring of fouling in hollow fiber membrane via UTDR, J. Membr. Sci. 326 (2009) 103–110.
[59] X. Li, J. Li, J. Wang, H. Wang, B. He, H. Zhang, Ultrasonic visualization of sub-critical flux fouilng in the double-end submirged hollow fiber membrane module, J. Membr. Sci. 444 (2013) 394–401.
[60] S.T.V. Sim, T.H. Chong, W.B. Krantz, A.G. Fane, Monitoring of colloidal fouling and its associated metastability using ultrasonic time domain reflectometry, J. Membr. Sci. 401–402 (2012) 241–253.
[61] G.Y. Chai, B. Cao, G.Y. Zhao, A.R. Greenberg, W.B. Krantz, Effects of concentration polarization, temperature and pressure on ultrasound detection of inor-

ganic fouling and cleaning in a spiral-wound membrane module, Desalin. Water Treat. 50 (2012) 411–422.
[62] X.Y. Lu, E. Kujundzic, G. Mizrahi, J. Wang, K. Cobry, M. Peterson, J. Gilron, A.R. Greenberg, Ultrasonic sensor control of flow reversal in RO desalination—Part 1: Mitigation of calcium sulfate scaling, J. Membr. Sci. 419–420 (2012) 20–32.
[63] G. Mizrahi, K. Wong, X.Y. Lu, E. Kujundzic, A.R. Greenberg, J. Gilron, Ultrasonic sensor control of flow reversal in RO desalination. Part 2: Mitigation of calcium carbonate scaling, J. Membr. Sci. 419–420 (2012) 9–19.
[64] J.S. Baker, L.Y. Dudley, Biofouling in membrane systems—A review, Desalination 118 (1998) 81–89.
[65] S.F.E. Boerlage, Scaling and Particulate Fouling in Membrane Filtration Systems, Taylor & Francis, London, 2001.
[66] R. Chan, V. Chen, Characterization of protein fouling on membranes: Opportunities and challenges, J. Membr. Sci. 242 (2004) 169–188.
[67] J.X. Li, R.D. Sanderson, G.Y. Chai, A focused ultrasonic sensor for in situ detection of protein fouling on tubular ultrafiltration membranes, Sensors Actuat. B: Chem. 114 (2006) 182–191.
[68] X.C. Xu, J.X. Li, N.N. Xu, Y.L. Hou, J.B. Lin, Visualization of fouling and diffusion behaviors during hollow fiber microfiltration of oily wastewater by ultrasonic reflectometry and wavelet analysis, J. Membr. Sci. 341 (2009) 195–202.
[69] X.H. Li, J.X. Li, J. Wang, H.W. Zhang, Y.D. Pan, In situ investigation of fouling behavior in submerged hollow fiber membrane module under sub-critical flux operation via ultrasonic time domain reflectometry, J. Membr. Sci. 411–412 (2012) 137–145.
[70] J.X. Li, R.D. Sanderson, G.Y. Chai, D.K. Hallbauer, Development of an ultrasonic technique for in situ investigating the properties of deposited protein during crossflow ultrafiltration, J. Colloid Interface Sci. 284 (2005) 228–238.
[71] S.K. Sikder, M.B. Mbanjwa, D.A. Keuler, D.S. McLachlan, F.J. Reineke, R.D. Sanderson, Visualisation of fouling during microfiltration of natural brown water by using wavelets of ultrasonic spectra, J. Membr. Sci. 271 (2006) 125–139.
[72] S.H.D. Silalahi, T. Leiknes, J. Ali, R. Sanderson, Ultrasonic time domain reflectometry for investigation of particle size effect in oil emulsion separation with crossflow microfiltration, Desalination 236 (2009) 143–151.
[73] E. Kujundzic, A.R. Greenberg, R. Fong, B. Moore, D. Kujundzic, M. Hernandez, Biofouling potential of industrial fermentation broth components during microfiltration, J. Membr. Sci. 349 (2010) 44–55.
[74] E. Kujundzic, A.R. Greenberg, R. Fong, M. Hernandez, Monitoring protein fouling on polymeric membranes using ultrasonic frequency-domain reflectometry, Membranes 1 (2011) 195–216.
[75] S.T.V. Sim, S.R. Suwarno, T.H. Chong, W.B. Krantz, A.G. Fane, Monitoring membrane biofouling via ultrasonic time-domain reflectometry enhanced by silica dosing, J. Membr. Sci. 428 (2013) 24–37.
[76] E. Kujundzic, A.C. Fonseca, E.A. Evans, M. Peterson, A.R. Greenberg, M. Hernandez, Ultrasonic monitoring of earlystage biofilm growth on polymeric surfaces, J. Microbiol. Meth. 68 (2007) 458–467.
[77] K. Cobry, Integrated Sensors for Real-time Monitoring of Membrane Performance During Nanofiltration, Mechanical Engineering, University of Colorado at Boulder, Boulder, CO, 2011.
[78] R.F. Probstein, K.K. Chan, R. Cohen, I. Rubenstein, Model and preliminary experiments on membrane fouling in reverse osmosis, in: A.F. Turbak (Ed.), Synthetic Membranes and Their Applications, American Chemical Society, Washington, DC, 1981, pp. 131–145.
[79] E.M.V. Hoek, J. Allred, T. Knoell, B.H. Jeong, Modeling the effects of fouling on full-scale reverse osmosis processes, J. Membr. Sci. 314 (2008) 33–49.
[80] J. Gilron, N. Daltrophe, M. Waissman, Y. Oren, Comparison between compact accelerated precipitation softening (CAPS) and conventional pretreatment in operation of brackish water reverse osmosis (BWRO), Ind. Eng. Chem. Res. 44 (2005) 5465–5471.
[81] J.S. Gill, A novel inhibitor for scale control in water desalination, Desalination 124 (1999) 43–50.
[82] D. Hasson, A. Drak, R. Semiat, Induction times induced in an RO system by antiscalants delaying CaSO4 precipitation, Desalination 157 (2003) 193–207.
[83] B.R. Breslau, A.J. Testa, B.A. Milnes, G. Medjanis, Advances in hollow fiber ultrafiltration technology. Ultrafiltration membranes and applications, in: A. Copper (Ed.), Polymer Science and Technology, Plenum Press, New York, NY, 1980, pp. 109–128.
[84] S. Hargrove, S. Ilias, Flux enhancement using now reversal in ultrafiltration, Sep. Sci. Technol. 34 (1999) 1319–1331.
[85] N. Pomerantz, Y. Ladizhansky, E. Korin, M. Waisman, N. Daltrophe, J. Gilron, Prevention of scaling of reverse osmosis membranes by "zeroing" the elapsed nucleation time. Part I. Calcium sulfate, Ind. Eng. Chem. Res. 45 (2006) 2008–2016.
[86] J. Gilron, M. Waisman, N. Daltrophe, N. Pomerantz, M. Milman, I. Ladizhansky, E. Korin, Prevention of precipitation fouling in NF/RO by reverse flow operation, Desalination 199 (2006) 29–30.
[87] M. Uchymiak, A.R. Bartman, N. Daltrophe, M. Weissman, J. Gilron, P.D. Christofides, W.J. Kaiser, Y. Cohen, Brackish water reverse osmosis (BWRO) operation in feed flow reversal mode using an ex situ scale observation detector (EXSOD), J. Membr. Sci. 341 (2009) 60–66.
[88] L. Lin, Z.M. Wang, M.L. Peterson, Conditions for bifurcation of the longitudinal wave in a porous medium, Acta Acust. United Ac 95 (2009) 373–378.
[89] L. Lin, In-situ Measurement of Permeability of a Porous Interface using the Ultrasonic Slow Wave, PhD Thesis, Department of Mechanical Engineering, University of Maine, Orono, 2011.
[90] J.C. Chen, Q.L. Li, M. Elimelech, In situ monitoring techniques for concentration polarization and fouling phenomena in membrane filtration, Adv. Colloid Interface 107 (2004) 83–108.
[91] V.L. Vilker, C.K. Colton, K.A. Smith, Theoretical and experimental-study of albumin ultrafiltered in an unstirred cell. 2, AIChE J. 27 (1981) 637–645.
[92] V.L. Vilker, C.K. Colton, K.A. Smith, An optical shadowgraph technique for measuring concentration

profiles near a solution-membrane interface. 1, AIChE J. 27 (1981) 632–637.
[93] C.R. Ethier, D.C. Lin, Refractometric measurement of polarized layer structure—studies of hyaluronic-acid ultrafiltration, J. Membr. Sci. 68 (1992) 249–261.
[94] W.D. Mores, R.H. Davis, Direct visual observation of yeast deposition and removal during microfiltration, J. Membr. Sci. 189 (2001) 217–230.
[95] M. Uchymiak, A. Rahardianto, E. Lyster, J. Glater, Y. Cohen, A novel RO *ex situ* scale observation detector (EXSOD) for mineral scale characterization and early detection, J. Membr. Sci. 291 (2007) 86–95.
[96] A.R. Bartman, E. Lyster, R. Rallo, P.D. Christofides, Y. Cohen, Mineral scale monitoring for reverse osmosis desalination via real-time membrane surface image analysis, Desalination 273 (2011) 64–71.
[97] H. Gu, A.R. Bratman, M. Uchymiak, P.D. Christofides, Y. Cohen, Self-adaptive feed flow reversal operation of reverse osmosis desalination, Desalination 308 (2013) 63–72.
[98] J. Thompson, N. Lin, E. Lyster, R. Arbel, T. Knoell, J. Gilron, Y. Cohen, RO membrane mineral scaling in the presence of a biofilm, J. Membr. Sci. 415 (2012) 181–191.
[99] H.G.L. Coster, T.C. Chilcott, A.C.F. Coster, Impedance spectroscopy of interfaces, membranes and ultrastructures, Bioelectroch. Bioener. 40 (1996) 79–98.
[100] H.G.L. Coster, K.J. Kim, K. Dahlan, J.R. Smith, C.J.D. Fell, Characterization of ultrafiltration membranes by impedance spectroscopy. 1. Determination of the separate electrical parameters and porosity of the skin and sublayers, J. Membr. Sci. 66 (1992) 19–26.
[101] K. Asaka, Dielectric-properties of cellulose-acetate reverse-osmosis membranes in aqueous salt-solutions, J. Membr. Sci. 50 (1990) 71–84.
[102] K.S. Zhao, M. Yasuhiro, K. Asaka, K. Asami, T. Hanai, Dielectric analysis of concentration polarization phenomena at cation-exchange membrane solution interfaces by frequency variation and dc bias application, J. Membr. Sci. 64 (1991) 163–172.
[103] T. Hanai, K.S. Zhao, K. Asaka, K. Asami, Dielectric theory of concentration polarization—relaxation of capacitance and conductance for electrolyte-solutions with locally varying conductivity, J. Membr. Sci. 64 (1991) 153–161.
[104] Y. Gao, W. Li, W.G.L. Lay, H.G.L. Coster, A.G. Fane, C.Y. Tang, Characterization of forward osmosis membranes by electrochemical impedance spectroscopy, Desalination, 312 (in press) 45–51.
[105] A. Antony, T. Chilcott, H. Coster, G. Leslie, *In situ* structural and functional characterization of reverse osmosis membranes using electrical impedance spectroscopy, J. Membr. Sci. 425 (2013) 89–97.
[106] K.D. Cobry, V.M. Bright, A.R. Greenberg, Integrated electrolytic sensors for monitoring of concentration polarization during nanofiltration, Sensor Actuat. B-Chem. 160 (2011) 730–739.
[107] A.R. Greenberg, J. Gilron, M.S. Mohsen, Novel High Recovery Desalination Process, in, NATO Report, 2012.